Annual Report on Contract NAS8-35354

SPACE RADIATION STUDIES

for the reporting periods
Nov 85-Feb 86; Mar-May 86; June-Aug 86, and Sept-Nov 86

Dr. J. C. Gregory
(205) 895-6028

Cosmic Ray Laboratory
School of Science
The University of Alabama in Huntsville
Huntsville, AL 35899

FINANCIAL STATUS REPORT

CONTRACT __NAS8-35354__

As of Feb. 16, 1987

Total Cumulative Costs incurred as of___$175,535.40_____

Estimate of cost to complete $221,780.00

Estimated Percentage of Physical Completion___79%_____

Statement relating the Cumulative cost to the percentage of physical
completion with explanation of any significant variance:

INTRODUCTION

The University of Alabama in Huntsville has provided instrument design and data analysis expertise in support of several of MSFC's space radiation monitoring programs. The Verification of Flight Instrumentation (VFI) program at NASA included both the Active Radiation Detector (ARD) (Principal Investigator: Dr. T. A. Parnell) and the Nuclear Radiation Monitor, (NRM), (Principal investigator: Dr. G. J. Fishman). The subject contract at UAH has provided design, partial fabrication, calibration and partial data analysis capability to the ARD program; and detector head design and fabrication, software development and partial data analysis capability to the NRM program.

The ARD flew on Spacelab-1 in 1983, performed flawlessly and was returned to MSFC after flight with unchanged calibration factors. The NRM, flown on Spacelab-2 in 1985, also performed without fault, not only recording the ambient γ-ray background on the Spacelab, as it was designed to do, but also recording radiation events of astrophysical significance.

RESULTS

1. The Nuclear Radiation Monitor

A Nuclear Radiation Monitor (NRM) was flown as part of the verification instrumentation on the Spacelab 2 mission, July 29 - August 6, 1985. The monitor is a 12.7 cm diameter, 12.7 cm thick NaI(Tℓ) scintillation detector surrounded by a charged particle detector. The NRM, mounted on a pedestal near the rear of the payload bay, has a nearly omnidirectional response. Gamma rays are detected with high efficiency over the energy range 0.06 to 30 MeV. The monitor operated throughout most of the mission, recording spectra every 20 seconds and counting rates in coarse energy bands on finer timescales.

The gamma radiation environment on Spacelab consists of cosmic-ray and trapped proton secondary radiation in the Spacelab/Shuttle, Earth albedo radiation, and delayed induced radioactivity in the detector and surrounding materials. Passages through the South Atlantic Anomaly protons produce a well-defined background enhancement. Episodes of greatly increased background due to trapped electrons are seen on many passes through high latitudes. This background has a soft spectrum, characteristic of bremstrahlung radiation. These enhancements often have complex temporal structure.

Many experiments on future Shuttle missions and other low-Earth orbit missions are sensitive to the ambient radiation environment. The Nuclear Radiation Monitor (NRM) was designed to measure various components of this environment on an early Shuttle/Spacelab mission. The primary objective of the instrument was to monitor the omnidirectional gamma-ray, proton, electron, and neutron fluxes over a wide energy range in the payload bay. These measurements are made in

conjunction with a more comprehensive, multifaceted program to characterize the Shuttle/Spacelab radiation fluxes and dosages. Data from the NRM will be made available to experimenters for the analysis and interpretation of their data and for the design of future Spacelab experiments.

1.a.   Background Gamma Radiation on Spacelab-2

The NRM operated throughout the mission and has provided a comprehensive time history and spectra data base for the entire flight. Gamma ray count-rates in various energy ranges, and coincidence count rates with the plastic scintillator shield (providing charged-particle count rates) have been analyzed. Variation with geomagnetic latitude and with such features as the south Atlantic anomaly and electron precipitations have been reported. This data was presented in a paper delivered by Dr. Paciesas at the 27th Plenary session of COSPAR at Toulouse, France, June 30 - July 12, 1986. A written version of this paper will appear in Advances in Space Research during 1987. The manuscript is reproduced in Appendix A of this report.

1.b.   Gamma-Ray Burst-Observed with the NRM

A strong gamma-ray burst fortuitously recurred during the Spacelab-2 mission and was detected and recorded by the NRM. A preliminary report of this observation was presented by Dr. G. J. Fishman at the Toulouse COSPAR meeting. Appendix B contains the written version of this paper entitled "Observation of a Strong Gamma Ray Burst on the Spacelab 2 Mission" to appear in 1987 in Advances in Space Research.

2. The Active Radiation Detector

Two tissue-equivalent integrating ion chambers and two xenon-filled proportional counters provided differential measurement of adsorbed dose and of particle count-rate for the Spacelab-1 mission. The record was not continous because of drop-outs in the data system. However data was obtained for 54% of the mission and sufficient orbital coverage was obtained to allow estimation of the total mission dose. These data have been combined with that from passive detectors flown by other investigators at MSFC and the VSF in the same mission. Papers presented by our coworkers including the ARD data were presented at the AIAA Meeting on Shutttle Environment and Operations, Houston TX November 1985 and at the 27th Plenary Meeting of COSPAR in Toulouse, France July, 1986. These two papers are reproduced in Appendices C of this report. The latter paper will appear in Advances in Space Science, 1987.

APPENDIX A

Measurements of Background Gamma Radiation on Spacelab 2

G. J. Fishman
Space Science Labortory
NASA Marshall Space Flight Center
Huntsville, AL   35812   USA

W. S. Paciesas
J. C. Gregory
University of Alabama in Huntsville
Huntsville, AL   35899   USA

Abstract

A Nuclear Radiation Monitor (NRM) was flown as part of the verification instrumentation on the Spacelab 2 mission, July 29 – August 6, 1985. The monitor is a 12.7 cm diameter, 12.7 cm thick NaI(Tℓ) scintillation detector surrounded by a charged particle detector. The NRM, mounted on a pedestal near the rear of the payload bay, has a nearly omnidirectional response. Gamma rays are detected with high efficiency over the energy range 0.06 to 30 MeV. The monitor operated throughout most of the mission, recording spectra every 20 seconds and counting rates in coarse energy bands on finer timescales.

The gamma radiation environment on Spacelab consists of cosmic-ray and trapped proton secondary radiation in the Spacelab/Shuttle, Earth albedo radiation, and delayed induced radioactivity in the detector and surrounding materials. Passages through the South Atlantic anomily protons produce a well-defined background enhancement. Episodes of greatly increased background due to trapped electrons are seen on many passes through high latitudes. This background has a soft spectrum, characteristic of bremsstrahlung radiation. These enhancements often have complex temporal structure.

INTRODUCTION

Many experiments on future Shuttle missions and other low-Earth orbit missions are sensitive to the ambient radiation environment. The Nuclear Radiation Monitor (NRM) was designed to measure various components of this environment on an early Shuttle/Spacelab mission. The primary objective of the instrument was to monitor the omnidirectional gamma-ray, proton, electron, and neutron fluxes over a wide energy range in the payload bay. These measurements are made in comjunction with a more comprehensive, multi-faceted program to characterize the Shuttle/Spacelab radiation fluxes and dosages (Parnell et al., 1986). Data from the NRM will be made available to experimenters for the analysis and interpretation of their data and for the design of future Spacelab experiments.

EXPERIMENT

The Nuclear Radiation Monitor (NRM) was flown in the payload bay of the Space Shuttle Challenger from July 29 to August 6, 1985, as part of the Spacelab 2 verification flight instrumentation. It operated continuously during the orbital portion of the flight. The Spacelab 2 mission had an orbital inclination of 49.5° and an altitude which varied between 290 km and 327 km during the flight.

The primary elements of the NRM detector assembly are shown in Figure 1. The NRM central detector is a 12.7 cm diameter, 12.7 cm thick NaI(Tℓ) scintillation crystal coupled to a 12.7 cm

scintillator, above a threshold of approximately 800 keV. Counts in these sixteen channels are accumulated in 8-bit scalers and read out every 5.25 ms. There are data gaps of 2.016 s duration every 20.16 s due to limitations of the data system.

A total of six spectra are accumulated for 18.144 s and read out every 20.160 s. Spectra of three different dispersions are accumulated from the central detector in coincidence with pulses from the plastic detector and three in anticoindicence with the plastic detector. The approximate dispersions are 1.5, 15, and 150 keV/channel in each spectrum of 510 channels.

The data system for the NRM represented the first use of the Spacelab Payload Standardized Modular Electronics (SPSME) components. These modules are CAMAC-compatible, space qualified electronics that can be configured and programmed for a variety of experiments and include appropriate interfaces to the Spacelab command, data, and power systems. The SPSME modules utilized for the NRM included a high rate multiplexer interface, a remote aquisition unit interface, a programmable crate controller, a time interface module, an auxilary memory module, an ADC module, and a power supply module. The total data rate from the NRM/SPSME was 24.381 kbps.

PRELIMINARY RESULTS

A portion of the data containing a strong gamma ray burst has been analyzed in some detail and the results are reported elsewhere (Fishman et al., 1986). Analysis of the remaining data has been oriented toward development of a comprehensive time

3

The remaining enhancements in Figure 2 represent background variations due to trapped electrons. These are only seen at high latitudes and have relatively soft spectra, as they are not prominent in the higher energy gamma ray channel. The gamma rays represent bremsstrahlung from the electron interactions in the atmosphere and the spacecraft. For the events in Figure 2, the electrons are not detected directly in the charged particle rate, probably due to the spacecraft orientation, since in other cases the charged particle rate has been seen to increase in coincidence with the soft-spectrum gamma ray rate increases.

Another feature of the electron events is the frequent occurrence of variations on timescales as short as 1 s, much faster than the proton events. Figure 3 shows one of these events with finer time resolution in the 100 - 600 keV gamma ray range. A rapid oscillation is seen in a portion of these data. Precipitation of energetic electrons at high latitudes with rapid, complex time structure has been observed and interpreted previously (cf. Barcus, Brown, and Rosenberg, 1966; Thorne and Kennel, 1971; Imhof et al., 1977; West and Parks, 1984; Imhof et al., 1986.).

Figure 4 shows a typical raw spectrum at the time of an electron event compared with a spectrum taken at a background minimum. The bremsstrahlung spectrum is relatively soft, the e-folding energy of the excess being ~100 keV. In contrast, the gamma-ray spectra of SAA passages typically differ from the low background regions in intensity but not in spectral shape. The spectral distinction of proton enhancements shows up primarily in the highest-energy charged particle spectra.

References

Barcus, J. R., R. R. Brown, and T. J. Rosenberg, "Spatial and Temporal Character of Fast Variatons in Auroral-Zone X-rays", J. Geophys. Res., 71, 125 (1966).

Fishman, G. J., "The Nuclear Radiation Monitor for the Spacelab/Shuttle", in Gamma Ray Spectroscopy in Astrophysics, NASA TM-79619, p479 (1978).

Fishman, G. J., W. S. Paciesas, C. A. Meegan, and R. B. Wilson, "Observation of a Strong Gamma Ray Burst on the Spacelab 2 Mission" (these proceedings) COSPAR Paper E.4.1.4 (1986).

Imhof, W. L., H. D. Voss, J. B. Reagan, D. W. Datlowe, E. E. Gaines, J. Mobilia, and D. S. Evans, "Relativistic Electron and Energetic Ion Precipitation Spikes Near the Plasmapause", J. Geophys. Res., 91, 3077 (1986).
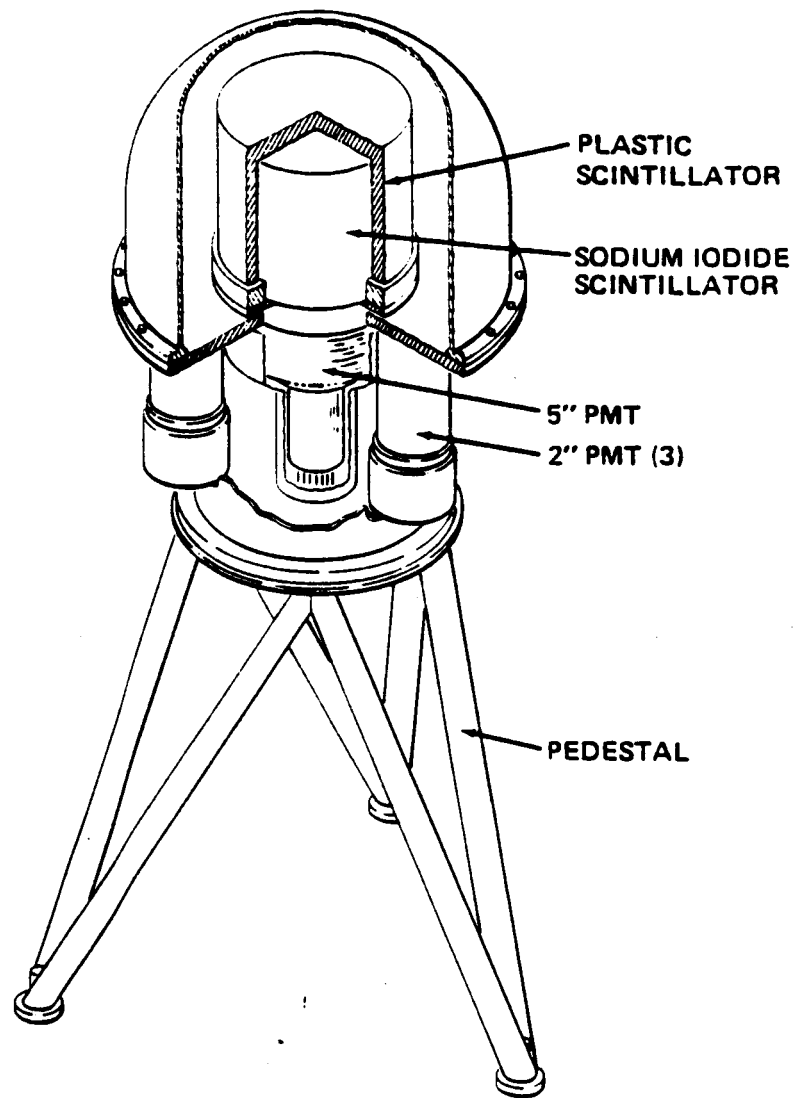
Imhof, W. L., J. B. Reagan, G. H. Nakano, and E. E. Gaines, "Narrow Spikes in the Selective Precipitation of Relativistic Electrons at Mid-Latitudes", J. Geophys. Res., 82, 117 (1977).

Parnell, T. A., J. W. Watts, G. J. Fishman, E. V. Benton, A. L. Frank, And J. E. Gregory, "The Measured Radiation Environment within Spacelabs 1 and 2 and Comparison with Predictions", (these proceedings) COSPAR Paper F.1.1.4 (1986).

PRECEDING PAGE BLANK NOT FILMED

Figure Captions

Fig. 1 The Nuclear Radiation Detector (NRM) on Spacelab 2. The primary detector components are indicated.

Fig. 2 Approximately 7.5 orbits of background data during the Spacelab 2 mission. Shown are the detected count rates in two gamma-ray energy regions and the integral counting rate from the scintillation detector in coincidence with the plastic scintillator. Several regions of increased background due to trapped electrons (E) and protons (SAA) are indicated, superimposed on the underlying modulation due to geomagnetic latitude variations. The time resolution of the data is 20.16 s.

Fig. 3 The low energy gamma ray counting rate during the time of an enhanced, variable electron background. The time resolution is 0.504 s.

Fig. 4 Spectrum of low energy gamma rays during an electron enhancement compared with a normal background spectrum. The energy scale is approximately 1.5 keV/chan.
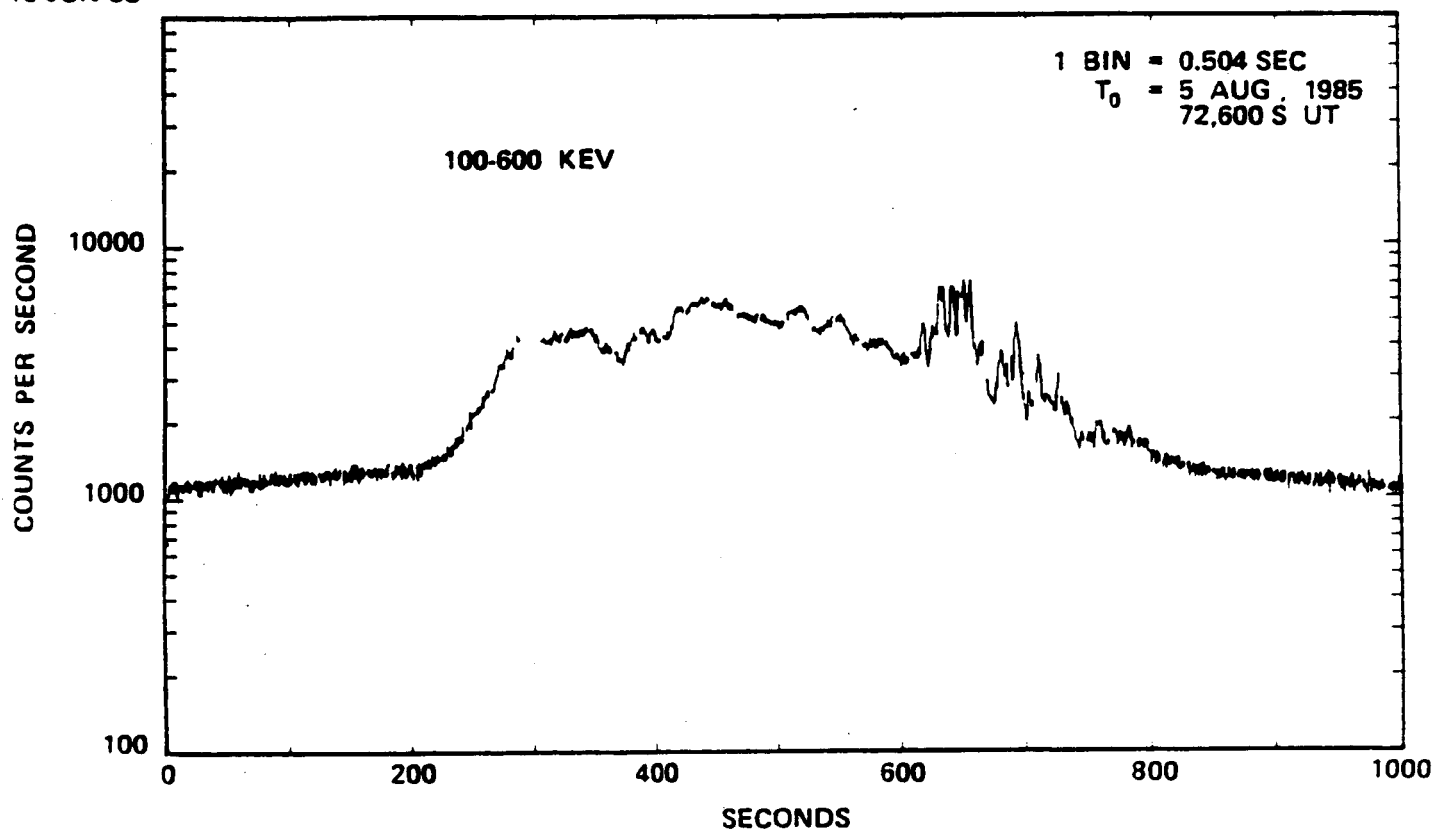
PLASTIC
SCINTILLATOR

SODIUM IODIDE
SCINTILLATOR

5" PMT

2" PMT (3)

PEDESTAL

NUCLEAR RADIATION MONITOR

Fig 1

Fig. 3

APPENDIX B

OBSERVATION OF A STRONG GAMMA-RAY BURST ON THE SPACELAB 2 MISSION

G. J. Fishman, W. S. Paciesas,[*] C. A. Meegan, and R. B. Wilson

Space Science Laboratory, NASA Marshall Space Flight Center,
Huntsville, AL 35812

ABSTRACT

A strong, confirmed gamma-ray burst was observed by a background-monitoring scintillation
detector on the Spacelab 2 mission. The peak of the burst was at 00:56:38 UT on August 5,
1985. The large size of the detector allowed observations up to 16 MeV with high
efficiency. A high data rate provided time-resolved observations over the energy range from
60 keV to 16 MeV, limited only by counting statistics.

The burst was dominated by a single peak, ~2 s wide, with softer, lower-level emission
lasting ~20 s after the main peak. There was no evidence for time structure less
than ~0.2 s anywhere in the burst in any energy range. These characteristics are similar to
a sizeable fraction (~25%) of bursts seen in the Konus catalog and we suggest that they are
distinct from the more complex, "spiky" bursts and may have a different emission mechanism.

In the energy range from ~560 keV to ~10 MeV, the burst peaks ~0.3 s before the peak at
lower energies. Radiation in the energy range ~10 to ~16 MeV was detected at a confidence
level of >96%, about 3 s before the lower energy radiation with roughly the same pulse
width. This radiation is not detected during the main part of the burst. The energy of
this burst in the range above 1 MeV is a significant fraction of the total burst energy,
confirming the earlier SMM results.

INTRODUCTION

It is now evident that gamma-ray emission from most bursts extends to energies well above 1
MeV and that this emission contains a significant fraction of the total burst energy
/1-3/. Thus it is increasingly important to obtain accurate spectral and temporal
characteristics of this radiation. The MeV emission has cast doubts on thermal radiation
being the dominant radiation process in these bursts. We report here the observation of MeV
gamma radiation from a burst on August 5, 1985. The availability of spectral information on
sub-second time scales has enabled us to observe significant differences in the burst time
history as a function of energy. These may have important implications for the development
of burst models.

EXPERIMENT

The Nuclear Radiation Monitor (NRM) was flown on the Spacelab 2 mission, July 29 to August
6, 1985. The objectives and details of this monitor are given elsewhere /4,5/. The central
detector is a 12.7 cm diameter, 12.7 cm thick NaI(Tl) crystal with a plastic anticoincidence
shield. The detector is uncollimated and has a low-energy threshold of 60 keV.

Scintillation pulses representing gamma rays were accumulated with 5.25 ms time resolution
in 12 energy regions. The first 11 energy regions were approximately logarithmically spaced
from 60 keV to 30 MeV. The last region was the integral energy region above 30 MeV. In the
lower energy regions, there were data gaps approximately 2 s in length every 20 s due to
limitations in the onboard data system. At higher energies, time resolution was lacking
during these same time periods. In addition to these 12 gamma-ray regions, there were
narrow-channel energy spectra accumulated with a time resolution of 20 s. The data from
these spectra are not used in the present burst studies due to their coarse time resolution.

[*]Also Physics Department, University of Alabama in Huntsville

ORIGINAL PAGE IS
OF POOR QUALITY

Prior to our own data analysis, we were notified of the occurrence of a strong gamma-ray burst on August 5 by the Los Alamos group (J. Laros, private comm.), who used data from the gamma-ray burst experiment on the Pioneer Venus Orbiter (PVO) spacecraft. The burst was found in our data at 00:56:38 UT on August 5, 1985. This time of occurrence was fortunate since the burst was not occulted by the Earth and Spacelab 2 was in a low-background portion of its orbit, the rate being ~1000 c/s above 60 keV. Subsequently, the burst was discovered in data from instruments aboard the International Cometary Explorer (ICE)(J. Laros, private comm.) and two other Spacelab 2 instruments: the cosmic-ray nuclei experiment (S. Swordy, private comm.) and the hard x-ray imaging experiment (G. Skinner, private comm.). We have verified that the burst time profiles from all five observations were similar.

Figure 1 shows the burst profile in five energy ranges, from 60 keV to 16 MeV. These counting rates are uncorrected for scattering and absorption by materials surrounding the detector and uncorrected for detector efficiency. Following the main peak, there is soft emission extending as a "shoulder" to the main peak for another 4 s. This shoulder is very prominent below 100 keV but is almost entirely absent above 560 keV. Additional soft features appear up to ~20 s beyond the primary peak. These features have time scales similar to the primary peak. No significant features are apparent on any time scale less than ~0.2 s in any energy interval. No precursor emission is seen at low energies. The peak of the emission in the energy range 560 keV to 2.8 MeV clearly precedes the lower energy peak by 0.3 s. There is no noticeable time delay between the peak at 100-560 keV and that below 100 keV. Significant emission in the energy region 2.8-10 MeV is also present. This radiation also peaks before the lower energy flux by ~0.5 s. Only a single, narrow peak ~1.0 s wide is evident in this energy region.

There is evidence for emission above 10 MeV from this burst, preceding the lower energy peak by approximately 3 s, as indicated in Figure 1. Figure 2 shows 200 s of data in two energy ranges, 100 to 560 keV and 10 to 16 MeV. In the high-energy region, the most prominent peak in this sample of data occurs 3 s before the low-energy peak. This peak is between 3 and 4 standard deviations above the background, depending on the bin width and phase.

The statistical significance of the emission in the energy range 10 to 16 MeV was estimated by Monte Carlo simulations of the data set. If we test the hypothesis that there is emission on the same time scale as the main peak at lower energies (~2 s) anywhere in the time interval within 5 s of this peak, then the region indicated in Figure 2 has a positive excess at the (99.3±0.1)% confidence level. If a more conservative view is taken, testing the hypothesis of emission on any time scale between 0.3 and 4 s at any time within 10 s of the peak, then the peak shown is significant at (96.9±0.6)% confidence level.

Based on time profiles alone, there may be a distinct class of gamma-ray bursts to which the August 5, 1985, burst belongs. This class has the following distinguishing characteristics: (1) a single peak, 2 to 6 s in duration, which dominates the time profile; (2) secondary features, if present, have roughly the same duration and typically follow the most intense peak; and (3) no time structure less than ~0.2 s is evident. The most complete set of data available for the comparison of time profiles is contained in the Konus catalog /6/. Since spectral information in that catalog is limited, it is not possible to determine whether the spectral characteristics
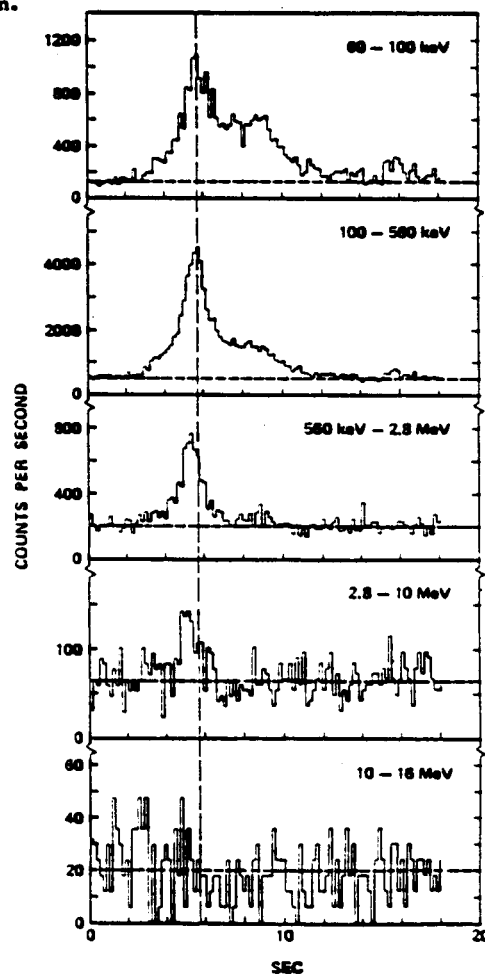

Fig. 1. Gamma-ray burst observed on Spacelab 2 in five energy regions with a time resolution of 0.168 s. The background levels in each region are indicated by a dashed line. The starting time of the plot is 00:56:33 UT, August 5, 1985.

observed in the present burst are common to the others as well. Figure 3 shows the profiles of some bursts of this class from the Konus catalog. Roughly 25% of all bursts in the Konus catalog may have the above characteristics. These bursts are contrasted with the "spiky" bursts which show complex time structure either as isolated spikes or as unresolved features in longer bursts with many fluctuations on a time scale of 0.2 s or less.
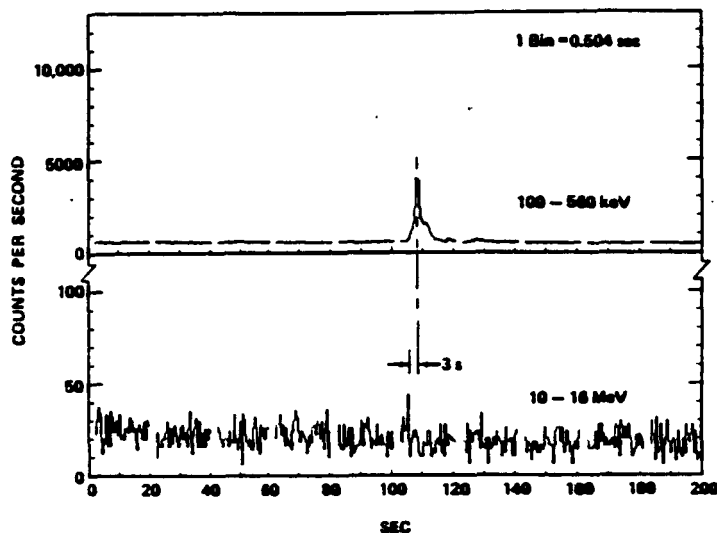
Fig. 2. Evidence for 10 to 16 MeV gamma-ray emission ~3 s prior to the peak of the low-energy emission. The statistical significance of this peak is discussed in the text. The peak occurs at t = 3 s in Figure 1.

TIME MARKERS = 5 SEC
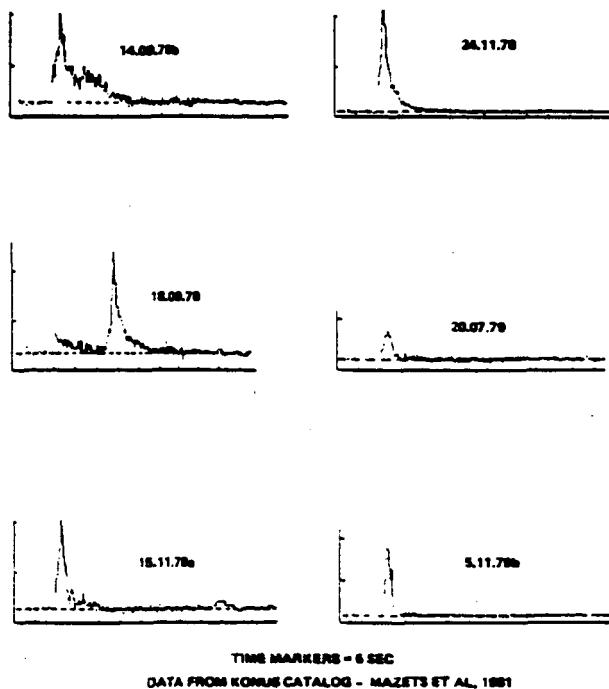DATA FROM KONUS CATALOG - MAZETS ET AL, 1981

Fig. 3. Examples of several single peak bursts from the Konus catalog from /6/. Time marks are shown every 5 s. The temporal structure of these bursts and the burst presented here are similar.

DISCUSSION

For the observed burst, we find that emission above 1 MeV represents an important component
of the total burst luminosity, confirming the earlier SMM results. In addition, the present
data have sufficient time and energy resolution to show that the MeV emission peaks earlier
than the lower energy flux. Preliminary estimates of the location (J. Laros, private comm.)
indicate that the burst was observed through the Shuttle, introducing significant scattering
and absorption. Nevertheless, it is apparent that the leading edge of the main peak of the
burst is very hard, also confirming the earlier SMM results. Later burst features are
softer; no significant emission is seen above 1 MeV. If the 10-16 MeV count rate excess
represents actual source flux, then the early portion of the burst is extremely hard since
the lower energy emission is just beginning to rise at that time.

These new results reinforce the importance of fine time resolution spectral studies of
bursts, particularly at high energies, as significant constraints for burst models /7,8/.
In particular, if the appearance of high-energy photons prior to those at low energies is an
ubiquitous feature of bursts or a class of bursts, current theoretical models may require
considerable revision.

REFERENCES

1. S.M. Matz, D.J. Forrest, W.T. Vestrand, E.L. Chupp, G.H. Share, and E. Rieger, High
   energy emission in gamma-ray bursts, Ap. J. Lett. 288, L37 (1985).
2. S.M. Matz, On the spectra of gamma-ray bursts at high energies, Ph.D. Thesis, University
   of New Hampshire (1986).
3. J.P. Norris, G.H. Share, D.C. Messina, B.R. Dennis, U.D. Desai, T.L. Cline, S.M. Matz,
   and E.L. Chupp, Spectral evolution of pulse structure in gamma-ray bursts, Ap. J. 301,
   213 (1986).
4. G.J. Fishman, The Nuclear Radiation Monitor for the Spacelab/Shuttle, in Gamma Ray
   Spectroscopy in Astrophysics, NASA TM-79619, p. 479 (1978).
5. G.J. Fishman, W.S. Paciesas, and J.C. Gregory, Measurements of background gamma radiation
   on Spacelab 2, this issue.
6. E.P. Mazets, S.V. Golenetskii, V.N. Il'Inskii, V.N. Panov, R.L. Aptekar, Yu.A. Gur'yan,
   M.P. Proskura, I.A. Sokolov, Z.Ya. Sokolova, T.V. Kharitonova, A.V. Dyatchkov, and N.G.
   Khavenson, Catalog of cosmic gamma-ray bursts from the KONUS experiment data, Astrophys.
   Space Sci. 80, 3 (1981).
7. I.G. Mitrofanov, V.Sh. Dolidze, C. Bara, G. Vedrenne, M. Neil, and K. Hurley, Rapid
   spectral variability of cosmic gamma-ray bursts, Sov. Astron. 28(5), 547 (1984).
8. E.P. Liang and V. Petrosian eds., Gamma Ray Bursts, AIP Conference Proceedings No. 141,
   AIP, New York 1986.

APPENDIX C

RADIATION ENVIRONMENT OF SPACELAB-1

E. V. Benton and A. L. Frank
University of San Francisco*

T. A. Parnell and J. W. Watts, Jr.
NASA-Marshall Space Flight Center

J. C. Gregory
University of Alabama, Huntsville

Abstract

The radiation environment of Spacelab-1 was measured by means of passive and active radiation detectors. Twenty-six passive detectors which were a part of the INS006 experiment were deployed inside the module and in the access tunnel between the module and crew compartment. Four other passive detectors which were a part of the Verification Flight Instrumentation (VFI) program were deployed in the module and outside on the pallet. The active detectors which were also a part of the VFI program included two integrating tissue equivalent ion chambers and two small Xenon-filled proportional counters placed in the module. Thermoluminescent detectors (TLD's) measured the low LET (linear energy transfer) component ranging from 94 to 133 mrads inside the module, yielding an average dose rate of 10.0 mrads per day, about twice the rate measured on earlier shuttle flights. Nuclear track detectors indicated substantial fluxes of highly ionizing HZE (high Z and energy) particles due to the higher inclination of the SL-1 orbit, which was 57° as opposed to 28.5° on previous shuttle flights. An average mission dose-equivalent rate of about 18.5 mrem/day was recorded which was approximately six times higher than measured on earlier missions. Neutron detectors indicated ~45 mrem for the flight. The two active ion chambers measured accumulated doses of 125 and 128 mrads and yielded 17 and 12 mrads for passages through the South Atlantic Anomaly (SAA). The proportional counters yielded up to 35 cps at northern latitudes due to cosmic rays, up to 200 cps in the middle of the SAA, primarily from protons, and up to 150 cps in the south horn of the electron belts, due primarily to brehmsstrahlung.

Introduction

In addition to personnel, the Spacelab missions incorporate many materials and experiments which are sensitive to the ionizing radiations found in Earth orbit. The radiation encountered is complex in particle type and energy spectra, reflecting its diverse origins. Primary galactic and solar cosmic rays as well as trapped protons and electrons produce secondaries such as recoil nuclei, nuclear reaction products and brehmsstrahlung through interaction with the materials of the spacecraft, its crew and its cargo. The fluxes and energy spectra are dependent on altitude and inclination of the orbit, on solar conditions, and the amount, type and placement of shielding materials in the spacecraft. Spacelab-1, flown on the STS-9 mission, orbited at an altitude of 241 km, with an inclination of 57° and 240 hours of flight time.

The inclination, considerably greater than for previous STS flights, was expected to result in substantially higher fluxes and dose rates of highly ionizing HZE particles as well as neutrons.

For the Spacelab missions in low Earth orbit, at low inclinations, the major components of the radiation are from the galactic cosmic rays and the energetic trapped protons. The HZE particles become more dominant as the orbital inclination is increased. At high altitudes, such as in a geosynchronous orbit, trapped electrons become important. The radiation hazard from large solar flare events becomes significant as the spacecraft orbits are increased in altitude and inclination and the geomagnetic shielding is correspondingly reduced[1,2]. This is the case for orbits of inclination greater than ~50°, polar and geosynchronous missions in which, particularly during EVA, potentially lethal doses of protons can be encountered. In addition to these naturally occurring radiations, spacecraft may encounter trapped electrons from high altitude nuclear tests as well as gamma rays and neutrons from on-board auxiliary power sources.

The various forms of radiation described above present a number of hazards to long-term space travel in an environment such as that of Spacelab. The highly penetrating nature of GCR makes it impractical to provide enough shielding to completely protect the crew. An indirect hazard also comes about from the effects of radiation on materials and electronics. Biomedical experiments in space may need to consider the possible effects of radiation. Although computer codes have been developed for calculating the environment inside the orbiting spacecraft in specific orbits, a number of uncertainties exist including those in the proton models (about a factor of 2), the electron belt models (about a factor of 5) and fragmentation cross sections of heavy ions [3,4]. Moreover, the shielding at any one location within the spacecraft is only approximately known and may vary with changes in the quantities and location of supplies and equipment, the movements of the crew, and the orientation of the spacecraft. The question of shielding poses one of the most difficult problems to solve in assessing radiation measurements.

Description of Instruments

Passive Detectors

This was the first attempt at mapping the radiation environment inside Spacelab. Measurements were made with a set of passive radiation detectors distributed throughout the volume inside the Spacelab-1 module, in the access tunnel and outside on the pallet.

Experiment INS006 detectors. Of the two different types of passive detectors selected for these measurements, twenty-six Passive Dosimeter Packets (PDP's) and four Thick Plastic Stacks (TPS's) were employed. The PDP's had dimensions of 8.6 cm x 6.6 cm x 0.2 cm and each contained a set of Types 200 and 700 TLD detectors for the overall low LET dose measurement and two layers of 1 mm-thick CR-39 plastic nuclear track detectors for the HZE particle measurement. Of these, 23 were deployed in the spacecraft while the other three were ground controls. The TPS's had dimensions of 9.8 cm x 9.8 cm x 5.2 cm and contained TLD's, CR-39 and AgCl crystals. Three were deployed in the module and one was used as a ground control. The AgCl detectors provided information on the fragmentation of galactic cosmic rays passing through spacecraft shielding as well as a better characterization of the directionality of the radiation field at given detector locations. The detectors were distributed over the inner surfaces of the Spacelab vehicle and the tunnel connecting to the crew compartment. The 26 locations represent a wide range of shielding distributions.

A sketch of the Shuttle cargo bay is given in Fig. 1, showing the locations of four PDP's at the Spacelab module end cones and two PDP's in the transfer tunnel. PDP's were also placed along the length of the module in sets of three as shown in Fig. 2, where a sketch of the module cross section at
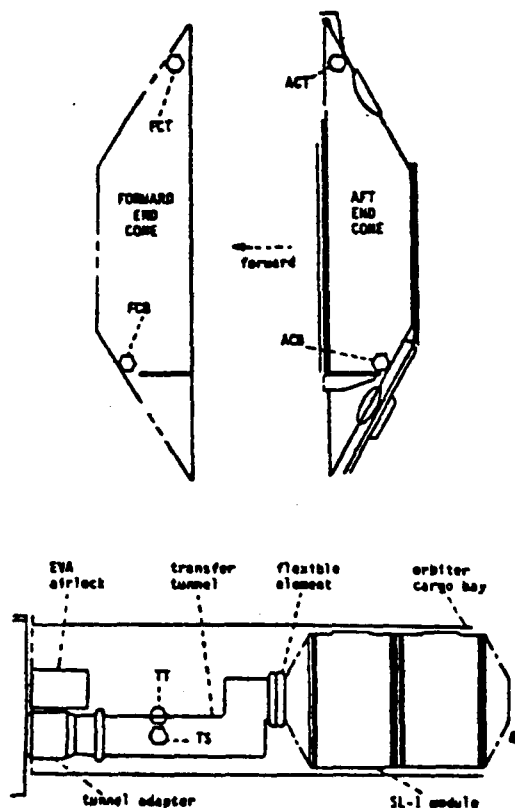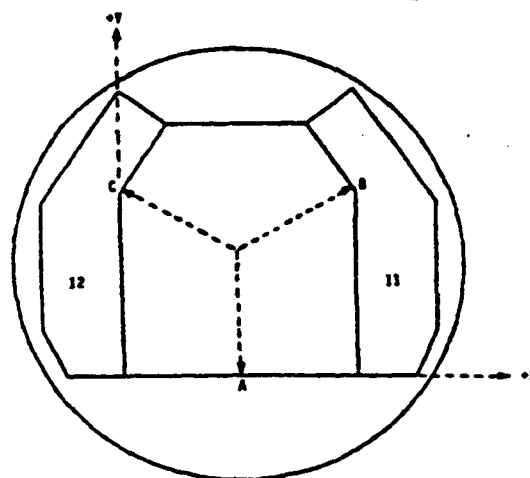
Fig. 2 Sketch of the view looking aft in the SL-1 module at Racks 11 and 12. The positions of PDP's A, B and C are denoted, as are the positive X and Y directions. The X, Y coordinates of the three PDP's are (1069, 0), (2107, 1813) and (32, 1813), respectively.

Racks 11 and 12 is given. The sets of three are spaced around the periphery of the module at five longitudinal distances. They are distributed at approximately equal radial angles, as in Fig. 2, but the angles are rotated with respect to the module structure. Of the TPS's, two were forward in the module at opposite sides and one was at the middle of the module.

VFI passive detectors. This set of detectors complemented the INS006 set. The detectors employed were CR-39 polycarbonate plastic pairs of sheets for HZE particles; CR-39 in conjunction with ^{6}LiF alpha-particle radiators, with and without Cd absorbers, for thermal (<0.3 eV) and resonance (0.3 eV-1 MeV) neutrons; mica in conjunction with ^{232}Th fission fragment radiators for high energy (>1 MeV) neutrons; nuclear emulsions for protons, and ^{7}LiF (TLD-700) and CaF_2 (TLD-200) thermoluminescent detectors for the total doses. The CR-39 and mica sheets are nuclear track detectors (NTD's) with sensitivities appropriate to the registration of the particles emitted by the corresponding radiators.

The detectors were distributed in two detector module types, PRD-M and PRD-P. Three PRD-M's were flown in the Spacelab module and one PRD-P on the pallet. The PRD-M's were identical except that only unit #3 contained neutron detectors. They were composed of stackable subassemblies of the same horizontal dimensions, with each subassembly containing a particular detector type. Each PRD-M was distributed in subassemblies, over three orthogonal inner sides of a PRD-M container, which was a larger box containing radiation detectors and sensitive materials. The distribution was as follows:

a) One LET stack subassembly, with its cover plate, positioned on the X-face of the PRD-M container.

b) The second LET stack subassembly, with its

Fig. 1 Sketches of the positions of the S1-1 module end cones, with the locations of PDP's TT, TS, FCT, FCB, ACT and ACB.

cover plate, positioned on the Y-face of the PRD-M container.

c) The third LET stack subassembly, with its cover plate and a TLD subassembly, positioned on the Z-face of the PRD-M container.

d) One nuclear emulsion subassembly positioned in the interior of the PRD-M container.

The PRD's also contained metal samples for the study of induced radioactivity from protons and neutrons. Photographic film samples were also included. Results from these measurements will be reported separately.

For the third PRD-M, the configuration was the same as the two identical PRD-M's, with the following addition: the LET stack subassembly positioned on the X-face of the PRD-M container had the neutron fission foil subassembly attached to it. This subassembly was sealed around the edges with "Aluminum Contact Tape." (Note: X, Y, and Z merely define orthogonal directions and should not be interpreted as referring to any fixed coordinate system.)

The PRD-P, which was mounted on the pallet, contained three parts from the University of San Francisco: TLD's for total dose, a thick cylindrical plastic stack for calculation of Z and LET spectra, and neutron fission foils for thermal, resonance, and fast neutron measurements. The subassemblies were cylindrically symmetrical and were aligned with the cylindrical axis of the PRD-P. A schematic drawing of a cross-section of the PRD-P is shown in Fig. 3.
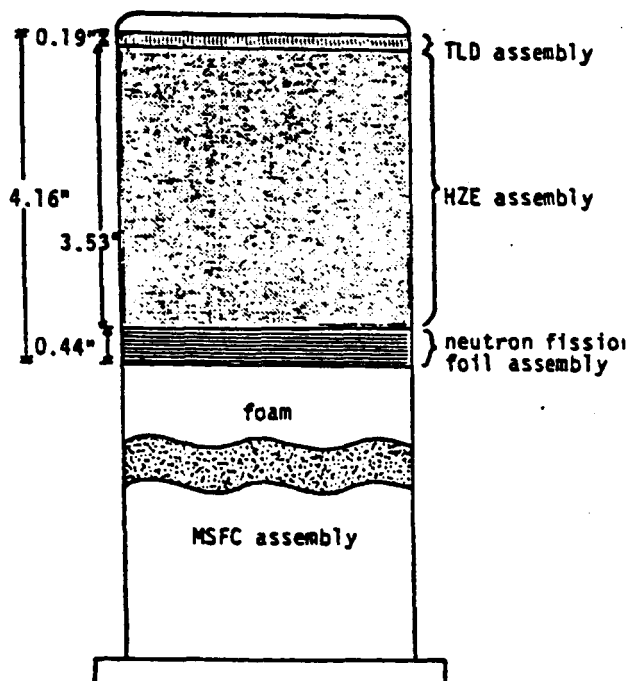
Fig. 3 Cross-sectional drawing of PRD-P

Active Detectors

The VFI also included two packages of active detectors (ARD's) which were designed to provide temporal information on the radiation in Spacelab.

and to the extent allowed by inexpensive and simple instruments, information about the main dose-contributing constituents. Each ARD package contained an integrating tissue-equivalent ion chamber and two small Xenon-filled proportional counters. The ion chamber[5] sensitive volume was a 7 cm diameter gas-filled sphere. It was similar to one flown on Skylab in the D008 experiment[6], but had a much higher sensitivity. The Spacelab units were set at about 10 μrads per integration. Fig. 4 shows an ARD package which has dimensions of 20 x 20 x 9 cm and weighs 2.5 kgm. The proportional counters were 2.5 cm diameter by 10 cm-long Xenon-filled units[7]. They are made from stainless steel cylinders and have a small beryllium window for calibration with low energy radioactive sources (e.g., ^{55}Fe). One of the counters was surrounded with a copper sleeve 1.2 mm thick. The data was read out each second through a Spacelab computer remote interface.
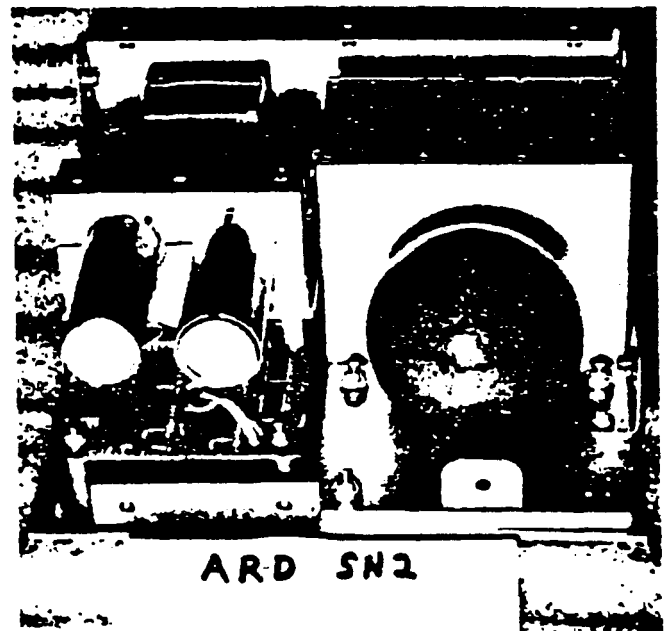
Fig. 4 Active Radiation Detector (protective cover removed)

The ion chamber responds to all ionizing radiation at approximately the same rate as tissue. The proportional counters respond to about 85% of all charged particles fast enough to penetrate the counter wall, and because they are filled with Xenon are also very sensitive to X-rays (brehmsstrahlung). An extensive preflight and postflight calibration program was carried out. Pre- and post-flight calibration values were in agreement within 5 percent. Ion chamber SN/1 which was located on top of Spacelab Rack No. 3 gave an output after each 6.1 ± 0.3μrads. SN/2 in the bottom of Rack 3 was set at 10.4 ± 0.5 μrads per count.

The proportional counter's discriminators were set for 5.9 keV whereas a fast proton (or electron) transiting the diameter would deposit 19.5 keV. The proportional counters' rates were about 1/sec on the ground.

Results

Passive Detectors

In Table 1 is listed the TLD-700 dose in mrads and the observed fluence of HZE particles as a function of spacecraft location. The overall absorbed dose varied from ~97 to 143 mrads inside the SL module. The observed HZE particle fluence varied from 125 to 435 tr/cm² in CR-39 for particles with LET∞ in water greater than ~48 keV/μm [8]. The correlation between dose and HZE fluence is poor, as seen in Fig. 5, where the two values have been plotted against each other for all the PDP's. Most of the TLD doses fall n the region from 100 to 115 mrads while the track fluences vary by a factor of 2.5 for these detectors. The two highest doses were recorded at the tops of the forward and aft end cones, which suggests less shielding at these sites. However, only the forward detector also had a higher-than-average number of HZE tracks.

Some preliminary angular shielding distributions have been generated for 23 of the PDP flight locations [9]. These distributions give the shielding mass thickness for 512 equal solid angle bins. Average shielding thicknesses have been calculated from these distributions and the TLD doses and HZE particle fluences are plotted against the average thicknesses in Figs. 6 and 7. The highest TLD doses (Fig. 6) were recorded by detectors which were among the least shielded, but the trend is not consistent. Without the two highest dose values, the profile of the measurements would be nearly flat. The HZE track fluences (Fig. 7) show a large scatter of the measured values with little correlation between the variables. In both figures the standard deviations about the linear regression lines and the correlation coefficients demonstrate the poor fitting. The mass thicknesses for the angular bins range from slightly over 1 gm/cm² to nearly 500 gm/

cm², although few values are over 180 gm/cm². The average shielding thicknesses calculated from the distributions are not distorted by a few high values, however, since all the PDP sites have a similar wide range of values. When TLD doses and HZE particle fluences are plotted against other shielding parameters, such as the fraction of total solid angle about the PDP sites which is lightly shielded (<12 g/cm²), there is little improvement in the correlation between measurements and shielding. This seems to indicate that other factors such as changes in spacecraft orientation with time and directionality of the incident radiation are also quite im-
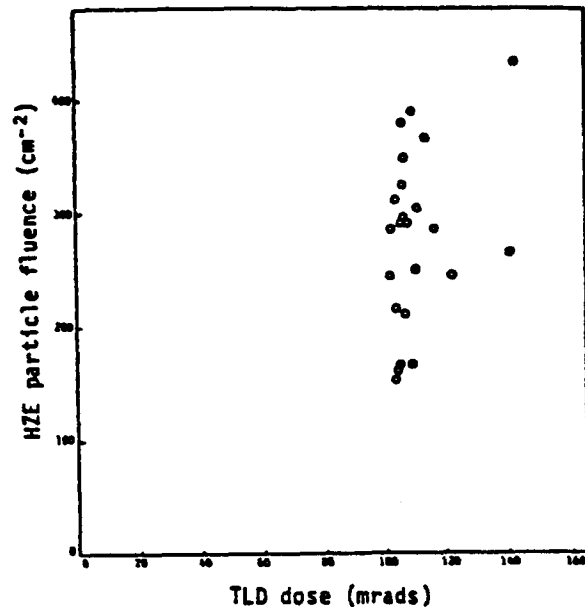

Fig. 5   A plot of the correlation between HZE particle fluences and TLD doses for the PDP's.

Table 1   Radiation measurement aboard Spacelab-1[14]

Detector location	TLD dose (mrad)	Observed HZE track fluence (cm⁻²)	Detector location	TLD dose (mrad)	Observed HZE track fluence (cm⁻²)
PORT SIDE			AFT END CONE		
B	113.8 ± 6.1	367 ± 55	ACT	141.0 ± 8.7	266 ± 41
D	106.6 ± 4.0	297 ± 47	ACB	102.5 ± 3.5	286 ± 39
G	103.5 ± 3.4	154 ± 20	FORWARD END CONE		
I	110.8 ± 3.4	250 ± 36	FCB	102.2 ± 2.7	245 ± 36
L	106.4 ± 2.7	326 ± 45	FCT	142.9 ±10.9	435 ± 59
N	107.0 ± 4.8	211 ± 28	SL-1 TUNNEL		
O	104.1 ± 2.8	313 ± 50	TS	122.3 ± 7.2	245 ± 36
P	105.1 ± 3.8	167 ± 25	TT	117.0 ± 4.5	286 ± 39
PRD-M1	97.1 ± 2.5	193 ± 28	OVERHEAD CONTAINER No. 7		
PRD-M3	109.1 ± 2.8	125 ± 19	PRD-M2	98.7 ± 2.5	180 ± 25
STARBOARD SIDE			PALLET		
C	111.0 ± 3.3	305 ± 45	PRD-P	189.8 ± 6.9	203 ± 26
E	106.3 ± 3.7	380 ± 53	TPS MEASUREMENTS		
F	106.9 ± 4.5	349 ± 38	PORT FORWARD		
H	109.2 ± 3.7	167 ± 25	FCR	102.0 ± 2.6	
J	109.7 ± 2.6	391 ± 58	STARBOARD FORWARD		
K	104.3 ± 3.1	161 ± 20	FCL	102.3 ± 4.1	
M	107.9 ± 4.0	292 ± 47	MIDDLE OF SPACELAB		
SL-1 FLOOR			DC	100.4 ± 1.5	
A	105.8 ± 2.6	292 ± 47	CREW COMPARTMENT STS-9		
Q	104.0 ± 2.8	216 ± 28	APD	103.2 ± 3.1	109 ± 13

4
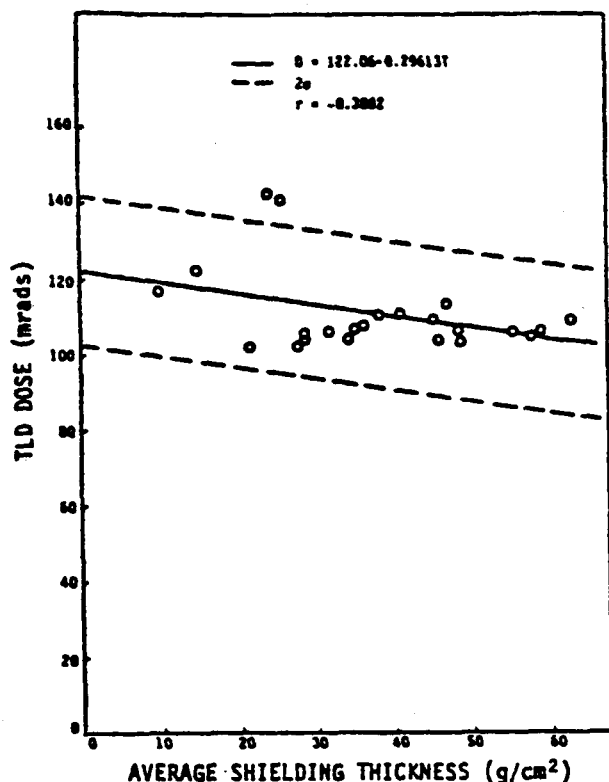
Fig. 6 Variations of the TLD (^{6}LiF) doses with average shielding thicknesses about the PDP's
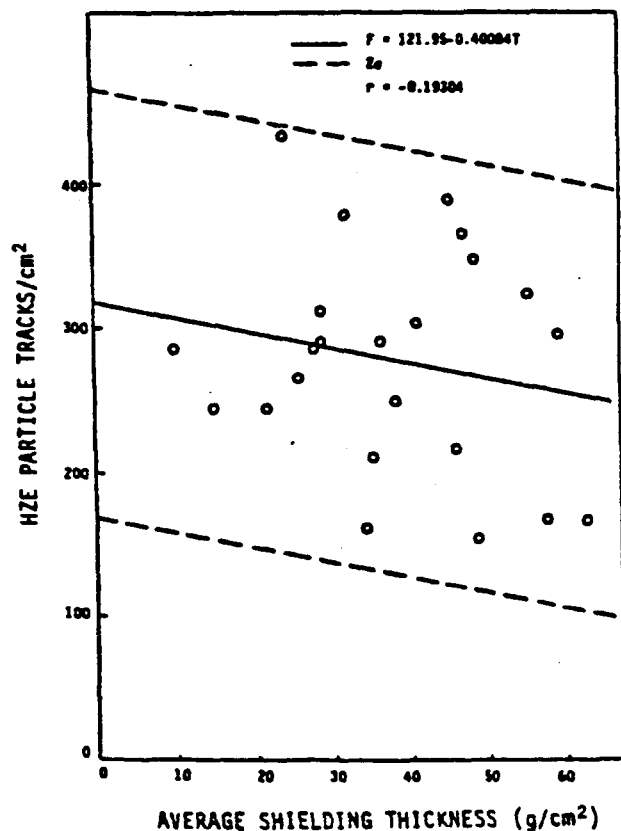

Fig. 7 Variation of the HZE particle fluences with average shielding thicknesses about the PDP's

portant to an understanding of the particular radiation levels.

An LET spectrum was generated from a population of particle tracks by measuring the major and minor axes of the elliptical openings of cones where two adjacent tracks formed when the particles passed through the interface of two CR-39 sheets.These measurements were converted to particle LET's by using calibrations of the CR-39 made with accelerated ion beams. The spectrum is plotted against log LET. in Fig. 8, where it is compared to other measurements. It is seen that the Spacelab-1 spectrum extends to much lower in LET than do previous measurements. This is an advantage of using the more sensitive CR-39 detectors.

The average TLD dose for the Spacelab module detectors listed in Table 1 was 108.2 ± 10.3 mrads. The average track fluence in the module was 265 ± 83 cm^{-2}. This track fluence converts to a dose equivalent of 185 ± 57 mrem, based on the LET spectrum and the relevant RBE values. From a calibration of TLD efficiency versus particle LET it has been calculated that the HZE particles contributed, on the average, 8.2 mrads to the TLD measured dose. The low LET dose measured by the TLD's (QF=1) was therefore 100.0 ± 10.3 mrads. By the same method the low LET doses found in the access tunnel and on the pallet were 111.4 ± 4.2 mrads and 184.3 ± 6.9 mrads, respectively. The corresponding high LET doses were 185 ± 18 mrem and 142 ± 18 mrem, respectively.

The proton track density was measured by the nuclear emulsions. The nuclear emulsion data is subject to greater measurement error than that of TLD's or NTD's. An average of the measurements yielded 4.61 ± 0.90 x 10^5 cm^{-2} for proton fluence and 2.61 ± 0.54 x 10^3 cm^{-2} for the fluence of particles with Z ≥ 2. In addition to the statistical standard deviations given, there are systematic errors present which may be of the order of ± 30%. It is interesting to note that the proton fluence, assuming an effective proton energy of 100 MeV, yields a tissue dose of about 55 mrads. This is somewhat less than would be expected from the TLD doses in the module, which are assumed to be dominated by the protons, but the experimental and calculational errors in this number are large enough that a rough agreement is indicated.

As stated above, the neutron detectors were composed of ^{6}LiF radiator foils in conjunction with CR-39 NTD's, and Th radiator foils in conjunction with mica NTD's. The ^{6}LiF/CR-39 detectors were used with and without 1 mm-thick Cd absorbers in order to discriminate between thermal (<0.3 eV) neutrons and resonance (0.3 eV—1MeV) neutrons. The Th/mica detectors measured the high energy (>1 MeV)neutrons.

The ^{6}LiF radiators were 4.5 mg/cm^2 in mass thickness. The 2π response to thermal neutrons is 5.6 x 10^{-3} alpha particle tracks/neutron from the front side (through the CR-39) and 4.1 x 10^{-3}tracks /neutron from the back side (through the ^{6}LiF). For a single film of ^{6}LiF against one surface of the CR-39, the averaged 4π response is 4.9 x 10^{-3}tracks /neutron. With films of ^{6}LiF in contact with both surfaces of the CR-39, each surface has a 4π response of 4.1 x 10^{-3}tracks/neutron. The CR-39/^{6}LiF detectors in the PRD-P had films of ^{6}LiF on both sides of the CR-39 NTD while those in the PRD-M had
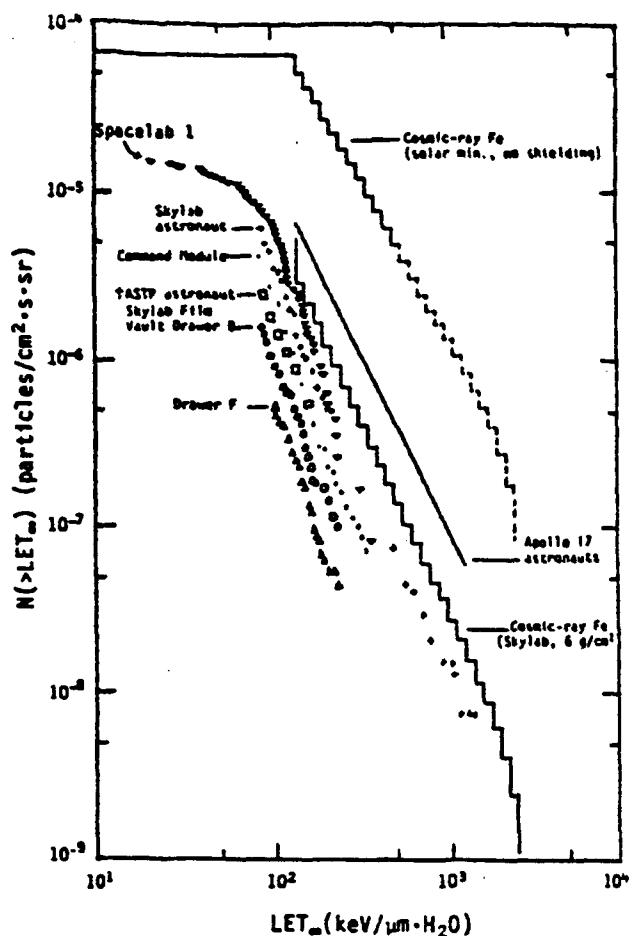
Fig. 8 Comparison of Spacelab-1 LET spectrum with other measured and calculated examples. The cosmic-ray Fe data were calculated. The earlier measurements were with Lexan polycarbonate and cellulose nitrate NTD's; CR-39 was used on Spacelab.

a single film. The response to resonance neutrons was calculated to be 2.15 x 10⁻⁴ alpha particle tracks/neutron, assuming a moderated neutron spectrum with a shape proportional to 1/En through the resonance energy range.

The Th radiators were approximately 0.13 g/cm² in mass thickness, which exceeds the ranges of the fission fragments produced by the interaction of high energy neutrons with the Th nuclei. The Th/mica detectors therefore have the maximum achievable sensitivity. These detectors are also sensitive to high energy protons, since protons of energy >17 MeV can produce nuclear fissions in Th. In determining the detector response to neutrons the proton contribution to measured track densities must be corrected for. An exact treatment of this problem requires that both the neutron and proton spectral shapes and their relative fluences be known. These properties and relationships were not measured on the Spacelab-1 mission. Assumptions were made based on past spaceflight measurements and on calculations of atmospheric spallation neutron spectra. Consequently there could be a large error in the calculated detector response. This method has been previously described [10,11] A response of 2.5 x 10⁻⁵ tracks/neutron was calculated for the Th/mica detectors, where the total track densities on the mica were used.

Only flight units PRD-M3 and PRD-P contained the neutron detectors. Ground control units were included for both flight units. These were used to provide the corresponding backgrounds for the flight measurements. After post-flight disassembly of the detectors the CR-39 and mica samples were etched and scanned at 200X under an optical microscope. Track densities were converted to neutron fluences and dose and the results are shown in Table 2, where the measured doses are summarized. The standard deviations of the measurements which are given in the table are from counting statistics only. The pallet detector indicates a more highly moderated neutron spectrum than does the module detector. This suggests that a large volume of hydrogenous material may have been placed near the pallet detector.

Active Detector Results

During the Spacelab-1 flight there were some data dropouts so the record was not continuous, but the orbit pattern repeats every day so that a mission dose was extracted. Data covering 54% of the mission was obtained. ARD SN/1 recorded a mission accumulated dose(extrapolated to total mission time) of 125 ± 7 mrads. SN/2 showed 128 ± 7 mrads. The experimental errors shown are calibration uncertainties only, and error sources such as temperature changes, long-term drift, and the data gap extrapolation are still being assessed.

The temporal information on dose contributions can be seen in Fig. 9 which shows the response of the ion chamber and proportional counters of ARD SN/1 during a period of the mission. Fig. 9 shows an hour of data which misses the trapped belt regions (either the SAA of the inner belt or cusps of the electron outer belt)[12]. Here it is seen that the dose rates and proportional counter rates vary slowly, and have a maximum value at north and south (geomagnetic) latitudes and a minimum near the equator. The main dose contribution here is due to the galactic cosmic radiation which is modulated by the Earth's field (geomagnetic cut-off). Fig. 10 shows an hour during which the orbiter passes through the center of the SAA region and shortly after leaving the SAA passes through a cusp of the electron belts. Early in the hour the proportional counters clearly show the high latitude cosmic ray induced rate followed by a low rate near the equator, a high rate in the SAA, and again a high rate in the electron belt horn. The ion chamber dose accumulation is high during the first 10 minutes (cosmic rays), low near the equator, very high during the SAA passage, and only slightly more than the cosmic ray accumulation during the electron cusp passes. The latter behavior is due to the sensitivity of the Xenon-filled proportional counters to brehmsstrahlung X-rays whereas the ion chamber is "tissue-equivalent" (of low atomic number absorber). The radiation inside the Spacelab module during the electron horn passes is apparently not the primary electrons but brehmsstrahlung X-rays caused by the electrons scattering in the module structure. The ratio of the shielded to the unshielded counter rates was near unity except during SAA and horn passages. During SAA passages there was a slight reduction in the shielded counter but during horn passage the ratio dipped as low as 0.6. This observation, and the ion chamber dose rate indicate that the main radiation constituents within Spacelab-1 are charged particles (protons)in the SAA passes and X-rays (brehmsstrahlung) during the electron horn passes.

Table 2   Summary of passive measurements*

	Fluence (cm^{-2})	Dose Equivalent (mrem)
Module TLD Low-LET		100.0 ± 10.3
Tunnel TLD Low-LET		111.4 ± 4.2
Pallet TLD Low-LET		184.3 ± 6.9
Module HZE High-LET	265 ± 83	185 ± 57
Tunnel HZE High-LET	266 ± 27	185 ± 18
Pallet HZE High-LET	203 ± 26	142 ± 18
Module Nuclear Emulsions		
Protons	4.61 ± 0.90 x 10^5	
Z > 2	2.61 ± 0.54 x 10^3	
Module Neutrons		
Thermal	1.1 ± 1.1 x 10^4	0.01 ± 0.01
Resonance	5.2 ± 1.6 x 10^5	2.5 ± 0.8
High-Energy	7.1 ± 0.6 x 10^5	42 ± 4
Pallet Neutrons		
Thermal	4.2 ± 1.3 x 10^4	0.04 ± 0.01
Resonance	1.5 ± 0.2 x 10^6	7.3 ± 0.8
High-Energy	7.6 ± 0.7 x 10^5	45 ± 4
Module Total Dose		330 ± 70
Pallet Total Dose		379 ± 46

*The errors of the constituent fluences and doses are those due to measurement statistics. The errors of the total doses are the best estimates of the total errors (σ).

ARD SN/2 shows a similar behavior, but the proportional counter rates are somewhat lower due to the shielding of the equipment and structure in Rack 3.

Discussion

The passive dosimeter results on Spacelab-1 showed some marked differences with measurements made in the crew compartments of previous STS flights and also with crew compartment measurements on STS-9. The low LET dose rate of 10.0 mrads/day is about twice the rate found on flights previous to STS-9, and nearly equal to that in the crew compartment of STS-9 (10.1 mrads/day)[13]. The high LET dose rate of 18.5 mrem/day is about six times higher than that four ' on earlier flights and also 2.4 times higher than found in the crew compartment (7.6 mrem/day) on the STS-9 mission. The total neutron dose of 4.45 mrem/day, in the module, is 2—4 times higher than found on the previous STS flights where similar measurements were made. There were no high energy neutron measurements made in the crew compartment on STS-9, but the resonance fluences measured there were approximately the same as in the module.

High energy neutron doses were not measured on the majority of the STS-missions, so a comparison of total doses cannot be made. On the basis of the low- and high-LET doses, however, the dose rate in the Spacelab module (28.5 mrem/day) is about 3.5 times higher than on previous flights and 1.6 times higher than in the crew compartment of STS-9.

A summary of some of the passive dosimetry data from U.S. manned spaceflights, including the TLD data from Spacelab-1, is given in Table 3. Data from several later STS flights are also included

for comparison. The variations of dose rates with the type of mission and with orbital parameters is clearly seen.

The ion chamber in SL-1 showed a mission accumulated dose of 125 ± (7+) mrads near the top of Rack 3 and 128 ± (7+) mrads in the bottom of Rack 3. The accumulated dose was mostly due to galactic cosmic rays and protons in the SAA. Ion chamber dose accumulation during passage through the SAA region was determined by choosing those segments of data where the proportional counter rate significantly increased and then determining the number of ion chamber counts in those regions. Ion chamber SN/1 accumulated 17 ± 1 mrads and SN/2 accumulated 12 ± 1 mrads during the SAA passes (extrapolated to total mission time). Since SN/2 is in a location with more effective shielding the relative dose indicates some absorption of the protons. These SAA doses are 13% and 10% of the total ion chamber dose respectively for periods when the data was available. Most of the remaining (tissue-equivalent) dose comes from the cosmic ray flux. The Xenon-filled proportional counters, which had a count rate of ~1 cps average on the ground, had count rates of up to 35 cps (av) at northern latitudes due to cosmic rays, up to ~200 cps (av) in the middle of the SAA (mostly due to protons and some X-rays) and up to 150 cps (av) in the south horn of the electron belts, primarily due to brehmsstrahlung X-rays produced by electrons in the Spacelab structure.

The detectors used in these measurements are responding to radiation that has been modified by the Spacelab and STS shielding. The cosmic rays are modified least. The SAA electrons and low energy protons are stopped by the structure and those remaining have their spectra modified. The intense electron flux in the horns is mostly absorbed in the
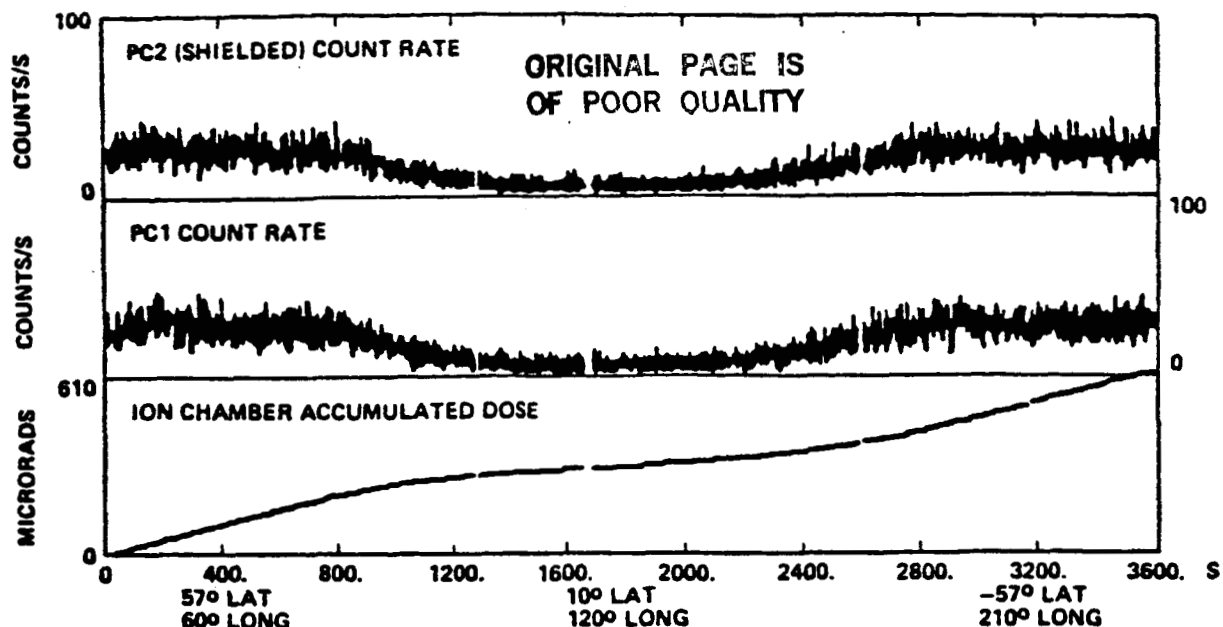
Fig. 9 Active radiation detector SN/1 response for one hour showing variations mostly due to galactic cosmic rays.
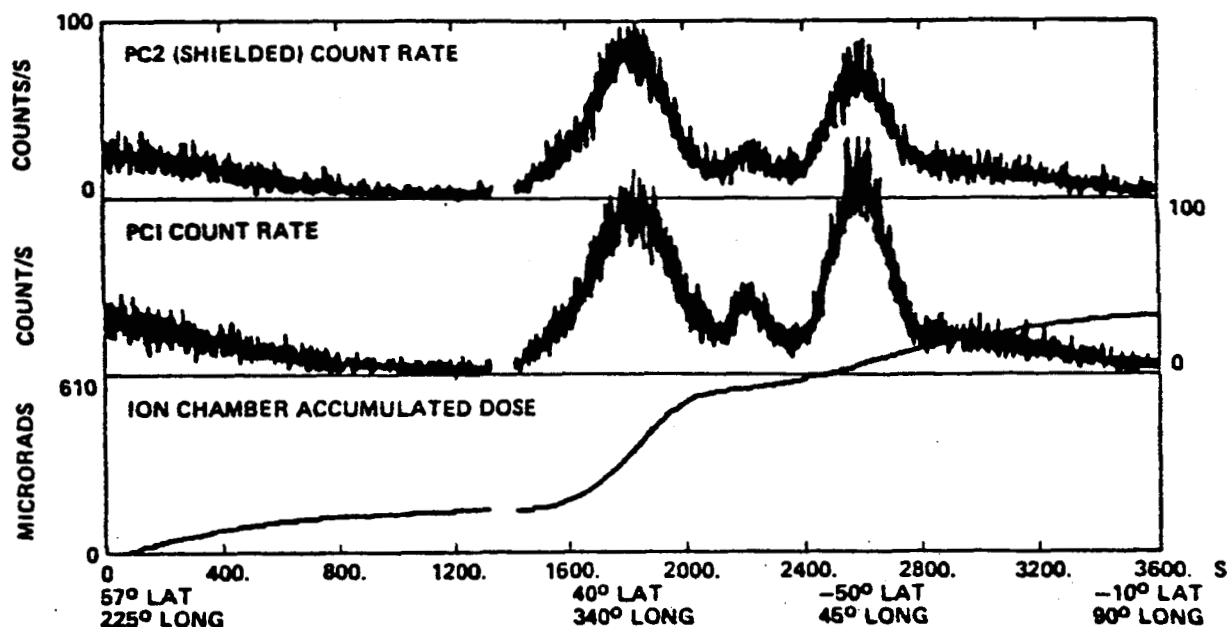
Fig. 10 Active radiation detector SN/1 response for one hour showing variations due to galactic cosmic rays, South Atlantic Anomaly particles and South Horn electrons.

SL structure but the brehmsstrahlung X-rays penetrate into Spacelab.

The mission dose and particle count rates on other missions will be quite dependent on the orbital parameters. The SAA proton flux increases rapidly with altitude[3], while the cosmic ray flux does not significantly increase. The fluence of the SAA particles is at a maximum around 40° orbital inclination where the spacecraft spends the maximum time in the Anomaly region. The cosmic ray flux will vary according to orbital inclination as

can be seen from Fig. 9. A 28.5° inclination orbit would have a much reduced cosmic ray component (GCR) to the dose. The electron belt horns would not be seen at inclinations below about 45° whereas at higher inclinations than 57° the brehmsstrahlung intensity would significantly increase.

The SL-1 active detectors give no information on individual components of the radiation such as neutrons or the heavy cosmic rays which produce the high LET tracks with their high relative biological efficiency. These detectors also produce no data

8

TABLE 3   Dosimetry Data from U.S. Manned Spaceflights

Flight	Duration (hrs/days)	Inclination (deg)	Apogee-Perigee (km)	Average Dose (mrad)	Average dose rate (mrad/day)
Gemini 4	97.3 hrs	32.5	296 - 166	46	11
Gemini 6	25.3 hrs	28.9	311 - 283	25	23
Apollo 7*	260.1 hrs			160	15
Apollo 8	147.0 hrs		lunar orbital flight	160	26
Apollo 9	241.0 hrs			200	20
Apollo 10	192.0 hrs		lunar orbital flight	480	60
Apollo 11	194.0 hrs		lunar orbital flight	180	22
Apollo 12	244.5 hrs		lunar orbital flight	580	57
Apollo 13	142.9 hrs		lunar orbital flight	240	40
Apollo 14	216.0 hrs		lunar orbital flight	1140	127
Apollo 15	295.0 hrs		lunar orbital flight	300	24
Apollo 16	265.8 hrs		lunar orbital flight	510	46
Apollo 17	301.8 hrs		lunar orbital flight	550	44
Skylab 2**	28 days	50	altitude ≈ 435	1596	57 ± 3
Skylab 3	59 days	50	" ≈ 435	3835	65 ± 5
Skylab 4	90 days	50	" ≈ 435	7740	86 ± 9
Apollo-Soyuz Test Project	9 days	50	" ≈ 220	106	12
STS-2†	57.5 hrs	38	" ≈ 240	12.5 ± 1.8	5.2
STS-3	194.5 hrs	38	" ≈ 240	52.5 ± 1.8	6.5
STS-4	169.1 hrs	28.5	" ≈ 297	44.6 ± 1.1	6.3
STS-5	120.0 hrs	28.5	" ≈ 297	27.8 ± 2.5	5.6
STS-6	120.0 hrs	28.5	" ≈ 284	27.3 ± 0.9	5.5
STS-7	143.0 hrs	28.5	" ≈ 297	34.8 ± 2.3	5.8
STS-8	70/75 hrs	28.5	" ≈297/222	34.8 ± 1.5	5.8
STS-9	240.0 hrs	57	" ≈ 241	101.1 ± 3.1	10.1
STS-9 (SL-1)				100.0 ±10.3	10.0
STS-41B	191.0 hrs	28.5	" ≈ 297	43.6 ± 1.8	5.5
STS-41C	168.0 hrs	28.5	" ≈ 519	403.0 ±12.0	57.6
STS-41D	145.0	28.5	" 297	42.0 ± 2.8	7.0
STS-41G	29/19/148.5	57.0	" 352/274/224	82.4 ± 2.4	10.0
STS-51A	192	28.5	" 324	94.3 ± 4.9	11.8

*Doses quoted for the Apollo flights are skin TLD doses. The doses to the blood-forming organs are approximately 40% lower than the values measured at the body surface.
**Mean thermoluminescent dosimeter (TLD) Skylab dose rates from crew dosimeters.
†STS data is an average of USF TLD-700 (^{7}LiF) readings.

on energy spectra of the radiation components, with the exception of some qualitative data on the brehmsstrahlung component, and SAA protons.

Conclusions

We have reported here the results of passive and active radiation measurements on SL-1 which provide the most comprehensive picture yet given of the radiation constituents in a large spacecraft in low Earth orbit. Because of its low altitude and short duration, Sl-1 was relatively benign in terms of total radiation dose. Some of the measurements such as the high-LET particles and neutrons have biological significance and potential effects on future experiments (e.g., gamma ray experiments) that are not at present fully assessed. The measurements clearly show the variety of phenomena that must be understood before extrapolation to other orbits or spacecraft shielding situations is possible, and before effects of long exposure at higher altitudes, such as in the space station, can be assessed.

References and Notes

1. D.M. Rust, Solar flares, proton showers and the Space Shuttle, Science 216, No.4549, 939-946 (1982).

2. E.V. Benton, Summary of current radiation dosimetry results on manned spacecraft, Adv. Space Res. 4, No.10, 153-160 (1984).

3. E.G. Stassinopoulos, The geostationary radiation environment, J. Spacecraft and Rockets 17, 145 (1980).

4. J.W. Watts, Jr. and J.J. Wright, Charged particle radiation environment for the Spacelab and other missions in low Earth orbit--Revision A. NASA Tech. Memo. TMX-73358, 1-137 (1976).

5. Digital Data Dosimetry, Tulsa, OK, Model 1/E-1.

6. G.C. Ainsworth, M.F. Schneider, J.F. Janni, A.D. Grimm, Skylab II—Radiation Dosimetry Systems and Flight Results, AFWL report AD-A032-409 (1976).

7. Reuter-Stokes, Cleveland, OH, Model RS-P3-0803-287.

8. The LET cut-off of 48 keV/μm for the type of CR-39 used may be refined in the future.

9. A. Hardy, W. Atwell and R. Beever, NASA-Lyndon B. Johnson Space Center, Houston, TX; private communication (1984).

10. E.V. Benton, R.M. Cassou, A.L. Frank, R.P. Henke and D.D. Peterson, Space radiation dosimetry on board Cosmos 936: U.S. portion of Experiment K-206, University of San Francisco TR-48 (1978).

11. E.V. Benton, R.P. Henke, A.L. Frank, C.S.Johnson, R.M. Cassou, M.T. Tran and E. Etter, Space radiation dosimetry aboard Cosmos 1129—Experiment K-309, University of San Francisco TR-53 (1981).

12. General description of Belts and Horns: see Refs. 3 and 4 above and also E.G. Stassinopoulos, NASA-SP 3054 (1970).

13. E.V. Benton, A.L. Frank, R.P. Henke, J.J. Almasi and R.M. Cassou, STS-9 Dosimetry Report, University of San Francisco TR-62 (1984).

14. The uncertainties shown are those due to counting statistics only; systematic errors resulting from a variety of factors may be as large as ± 30%.

THE MEASURED RADIATION ENVIRONMENT WITHIN SPACELABS 1 AND 2 AND COMPARISON WITH PREDICTIONS

T. A. Parnell,* J. W. Watts, Jr.,* G. J. Fishman,*
E. V. Benton,** A. L. Frank,** and J. C. Gregory***

*NASA Marshall Space Flight Center, Huntsville, AL 35812, U.S.A. **Department of Physics, University of San Francisco, San Francisco, CA 94117, U.S.A. ***Department of Chemistry, University of Alabama in Huntsville, Huntsville, AL 35899, U.S.A.

ABSTRACT

To measure the radiation environment in the Spacelab (SL) module and on the pallet, a set of passive and active radiation detectors was flown as part of the verification of flight instrumentation (VFI). SL1 carried 4 passive and 2 active detector packages which, with the data from the 26 passive detectors of Experiment INS006, provided a comprehensive survey of the radiation environment within the spacecraft. SL2 carried 2 passive VFI units on the pallet. Thermoluminescent dosimeters (TLD's) measured the low linear energy transfer (LET) dose component; the HZE fluence and LET spectra were mapped with CR-39 track detectors; thermal and epithermal neutrons were measured with the use of fission foils; metal samples analyzed by gamma ray spectroscopy measured low levels of several activation lines. The TLD's registered from 97 to 143 mrad in the SL1 module. Dose equivalents of 330±70 mrem in the module and 556±37 mrem on the SL2 pallet were measured. The active units in the SL1 module each contained an integrating tissue-equivalent ion chamber and two differently-shielded xenon-filed proportional counters. The ion-chambers accumulated 125 and 128 mrads for the mission with 17 and 12 mrads accumulated during passages through the South Atlantic Anomaly (SAA). The proportional counter rates (~1 cps at sea level) were ~100 cps in the middle of the SAA (mostly protons), ~35 cps at large geomagnetic latitudes (cosmic rays) and ~100 cps in the South Horn of the electron belts (mostly bremsstrahlung). Detailed results of these measurements and comparison with calculated values from radiation environment and shielding models are described.

INTRODUCTION

The radiation environment within the Spacelab module and on the pallet are of interest to many who will use the facility. The biomedical community, gamma ray astronomers and others with radiation sensitive detectors, experimenters with photographic material, those with instruments containing many microcircuits sensitive to "single event upsets," etc. need the radiation to be characterized. Since the ambient cosmic ray and trapped belt radiation is considerably modified by the shielding of the Spacelab and the shuttle mass, and some constituents are produced by interactions, predicting the complete radiation environment within the lab would be a formidable problem. Uncertainties in the trapped proton flux (~ factor 2) and electrons (~ factor 5) currently exist. The cosmic rays interact with the structure producing a variety of secondary particles and fragmenting the heavy nuclei. Some trapped protons are absorbed or interact producing neutrons, target spallation products, or recoil nuclei. The trapped electrons are mostly absorbed in the structure, but generate penetrating bremsstrahlung photons. Predicting the radiation is further complicated by the complex shielding distributions, by various attitudes of the spacecraft in the somewhat directional primary radiation field, and changing shielding due to consumables and equipment or crew movements.

The initial step in fulfilling future user's need for radiation environment information on Spacelab (SL) were the preflight predictions /1/ and the radiation measurements performed on SL1 and SL2. The predictions used simplifed shielding distributions and predicted only rad lose and the fluence of protons and electrons as a function of shield thickness.

The measurements were performed both by selected experiments (principally INS006 on SL1) and by instruments of the Verification Flight Instrumentation (VFI) Program on SL1 and SL2. Measurements were made with passive detectors of total mission lose, heavy nuclei fluence and linear energy transfer (LET) spectra, neutron fluence, activation of metal samples, and effects on photographic and nuclear track emulsions. Simple electronic detectors were used on SL1 to determine temporal variations of dose and count rate due to

cosmic rays and trapped protons and electrons. SL2 also carried a gamma ray spectrometer (the Nuclear Radiation Monitor) in the VFI program which measured the gamma ray background spectrum and its temporal behaviour in the payload bay. Results from it are discussed in paper XII.2.7, this conference. This set of measurements covered many of the phenomena required to characterize the radiation environment within a complex spacecraft, and offers a large set of data to compare with calculations from radiation models.

In this paper we present results of radiation dose measured with thermoluminescent dosimeters (TLD's) and ion chambers, and compare them with preflight predictions and postflight calculations using actual shielding distributions. The electronic detector results on temporal variations, and conclusions about the principal dose constituents are discussed. The heavy ion and neutron fluence and the biological dose equivalent (rem) measured with CR-39 nuclear track detectors and neutron fission foil detectors are presented. Postflight measurements of residual induced activity in the activation metal samples are discussed. Results from the exposure of nuclear track emulsions and photographic materials will be reported separately. The preflight predictions and recent calculations using actual shielding distributions are compared with the measurements. Implications for future radiation prediction programs (e.g., for the space station) are discussed.

INSTRUMENTS AND TECHNIQUES

The measurements reported here are from 26 passive detector packages of SL1 experiment INS006 /2/, 4 passive and 2 active detector packages of the VFI program /3/ on SL1, and 2 passive VFI packages on SL2. The instruments are summarized in Figure 1.

The INS006 experiment packages were in 2 configurations. Twenty-three Passive Dosimeter Packets (PDP's) and 3 Thick Plastic Stacks (TPS) were flown. The PDP's contained a set of LiF thermoluminescent dosimeters (TLD's) type 700 and CaF_2 type 200 for low linear energy transfer (LET) dose measurements and two 1 mm thick sheets of CR-39 nuclear track

detectors for HZE (heavy ion) measurements. The TPS packages contained TLD's, CR-39

sheets; and AgCl crystal track detectors to extend the measurement of HZE particles below

the threshold of the CR-39 detectors. The CR-39 detectors had a normal incidence

threshold of $LET_{\infty}(H_2O) = 40$ keV/µm equivalent to minimum ionizing $Z = 15$. The threshold

was 8 keV/µm and $Z = 7$ for SL2. The INS006 packages were distributed at various locations

within the Spacelab module and in the access tunnel to the shuttle crew compartments.

These locations were at a wide range of average and minimum shielding which are further

described in reference /4/ and section IV.
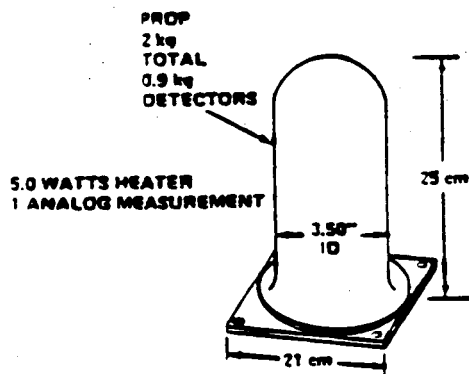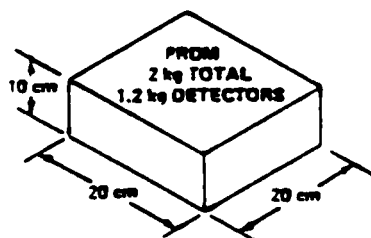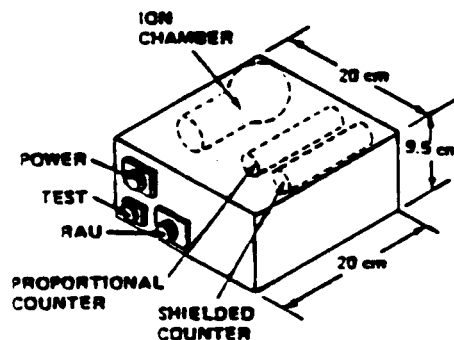
Fig. 1. Detector package configurations for Experiment INS006 and Verification Flight Instrumentation on Spacelab 1.

The VFI passive radiation detector (PRD) packages were in two configurations. The passive radiation detectors on the pallet (PRD-P's) were in hermetrically sealed cylindrical containers. The passive radiation detectors in the module (PRD-M's) were in sheet metal boxes. SL1 carried three PRD-M's and one PRD-P. SL2 carried two PRD-P's. The PRD's all contained TLD's for low LET total dose, CR-39 for HZE measurements, photographic film, and nuclear track emulsion samples. One PRD-M and the PRD-P on SL1 and one PRD-P on SL2 contained fission foil neutron detectors and metal activation samples. The PRD-P's contained discs of CR-39 and other detector arrays 8 cm in diameter. Each PRD-M contained three orthagonally placed subassemblies of HZE detectors consisting of sheets of CR-39, 2 x 58 cm^2 in area. The CR-39 threshold is incident angle dependent and this arrangement allows the omnidirectional HZE fluence and directional dependence to be sampled.

The neutron detectors employed CR-39 track detectors in contact with ^{6}LiF alpha radiators, with and without Cd absorbers, for discriminating thermal (<0.3 eV) and resonance (0.3-1 MeV) neutrons. Mica track detectors were placed in contact with Th fission fragment radiators to measure >1 MeV neutrons. For single interface detectors the response of the ^{6}LiF/CR-39 detectors was calculated to be 4.3 x 10^{-3} $\frac{1}{}$tracks in CR-39/thermal neutron and 2.15 x 10^{-4} x tracks in CR-39/resonance neutron (assuming a moderated 1/En neutron spectrum through the resonance energy region). The high energy detectors were also sensitive to protons above 17 MeV which can cause fission in Th. Deriving the high energy neutron fluence requires assumptions about the proton and neutron fluences and spectra, which cause uncertainties in the results. The method used here has been previously described /5,6/. A response of 2.5 x 10^{-5} fission fragment tracks in mica/high energy neutron was calculated. Further details of the neutron detectors are in Reference 4.

The two VFI Active Radiation Detector (ARD's) packages on SL1 each contained an integrating tissue-equivalent ion chamber /7/ and two xenon-filled proportional counters /8/. These rather simple omnidirectional detectors were designed to measure temporal variations of radiation dose and count rate due to cosmic ray nuclei, trapped protons and electrons, and bremsstrahlung x-rays from electrons stopped in the SL structure. The ion

5

chambers had a sensitive gas volume of 180 cm^3. Preflight calibrations of the ion chambers at 6.1 ± 0.3 μrads and 10.4 ± 0.5 μrads per unit output were reproduced after the flight within 5%. The proportional counters (PC's) had a sensitive volume of ~60 cm^3 and counted each ionizing event with energy deposition greater than 5.9 keV in the gas (about 35% of the charged particles and 2% of 100 keV photons are counted). In the laboratory the PC's count rate was ~1/sec. One PC of two in each unit was surrounded by a copper sleeve 1 g/cm^2 thick which would absorb >40% of 100 keV photons. The ARD's were placed in the top and bottom of equipment rack 3 in the SL1 module. A PRD-M was placed beside each ARD.

Results of Measurements

The Spacelab 1 mission flew for 10 days at ~250 km altitude and 57° inclination. Twenty-nine passive and two active detector packages were used at a variety of shielding locations in the module and tunnel, and one PRD-P was on the pallet. Spacelab 2 flew at ~315 km, 49.5° inclination for 3 days. Two PRD-P packages with almost identical shielding were in the payload bay. We first summarize the measurements of total radiation dose with the TLD's and ion chambers, and then discuss the temporal behavior of the dose and count rate from the active detectors. Next the HZE particle and neutron fluences and the mission biological dose are presented, and finally activation of metal samples is discussed. Table 1 summarizes the results.

The Spacelab 1 TLD's in the module registered low LET doses ranging from 9.7 ± 0.3 to 14.3 ± 1.1 mrads/day (total registered dose divided by 10). The average in the module was 10.0 mrads/day. The TLD's in the PRD-P behind 1.0 g/cm^2 minimum shielding registered 19.0 ± 0.7 mrads/day. On SL2 the two sets of TLD's in the payload bay behind 1.25 g/cm^2 minimum shielding registered 31.9 ± 1.6 and 31.0 ± 1.5 mrads/day. The location of individual measurements is further described in reference 4 and the sample shielding distributions and comparison with environment calculations are discussed in the next section.

6

The ion chamber dose measurements had many data gaps, but 54% of the mission was covered. The average dose rates were 12.5 ± 0.7 and 12.3 ± 0.7 mrads/day in the top and bottom of rack 3. TLD measurements in adjacent PRD-M's registered 9.7 ± 0.3 mrad/day and 10.9 ± 0.3 mrad/day, respectively. The ion chambers thus appear to measure about 20% higher values than the TLD's. Part of this is due to the TLD's lower sensitivity to heavy nuclei. As discussed later, about 85% of the SL1 module dose comes from cosmic rays, and the TLD's are less sensitive to very heavy nuclei than singly charged particles. An exact calculation of the expected difference would require a transport calculation for the heavy nuclei including slowing and fragmentation, which has not been done. A simplified estimate using the primary cosmic ray relative abundances in magnetic rigidity and a TLD dose calibration with heavy ions /9/ indicates about 15% difference. Other potential contributions are systematic biases in calibration and biased environment sampling due to data gaps.

The temporal information from the ion chambers and proportional counters allowed an assessment of the relative contributions of the cosmic rays and trapped belt particles. Figure 2 is a 1-hour segment of data from one ion chamber and the two PC's in the same unit. This shows variations in ion chamber dose integration and proportional counter rates due to cosmic rays (with the expected geomagnetic dependence); and the trapped particles in the South Altantic Anomoly (SAA) region and the south "horn" of the electron belt. The observation that the ion chamber dose rates in the south-horn region are not significantly different from rates at other high latitude portions of the orbit suggest that the high proportional counter rates there are due to bremsstrahlung photons produced by electrons stopping in the spacelab structure. The high proportional counter rates in the SAA are due to the trapped protons that produce the increase in IC dose rate in that region. The relative absorption efficiency of photons in the low atomic number gas in the tissue-equivalent ion chamber and high atomic number gas (xenon) in the proportional counters enables this distinction in the measurements.

7

TABLE 1 Summary of Measurements on SL1 and SL2

	Fluence (cm^{-2})	Dose Equiv. (mrem)
SL1 (10 Days)		
Module TLD low-Let (average)		100.0 ± 10.3*
Tunnel TLD low-LET (average)		111.4 ± 4.2*
Pallet TLD low-LET		184.3 ± 6.9*
Module TLD low-LET (range)		97 to 143
Module HZE high-LET ‡	265 ± 83	185 ± 57
Tunnel HZE high-Let ‡	266 ± 27	185 ± 18
Pallet HZE high-LET ‡	203 ± 26	142 ± 18
Module nuclear emulsions		
Protons	$4.61 ± 0.90 \times 10^5$	
Z > 2	$2.61 ± 0.54 \times 10^3$	
Module neutrons		
Thermal	$1.1 ± 1.1 \times 10^4$	0.01 ± 0.01
Resonance	$5.2 ± 1.6 \times 10^5$	2.5 ± 0.8
High-energy	$7.1 ± 0.6 \times 10^5$	42 ± 4
Pallet neutrons		
Thermal	$4.2 ± 1.3 \times 10^4$	0.04 ± 0.01
Resonance	$1.5 ± 0.2 \times 10^6$	7.3 ± 0.8
High-energy	$7.6 ± 0.7 \times 10^5$	45 ± 4
Module total dose		330 ± 70
Pallet total dose		379 ± 46
Ion chamber SN1		125 ± 7*
Ion chamber SN2		128 ± 7*
PC1 unshielded (10-150 cps)		
PC1 shielded (10-110 cps)		
SL2 (8 Days)		
Pallet TLD low-LET		245 ± 12*
Pallet HZE high-LET ‡	493 ± 46	269 ± 25
Pallet neutrons		
Thermal	$1.4 ± 0.3 \times 10^5$	0.14 ± 0.03
Resonance	$2.0 ± 0.4 \times 10^6$	9.7 ± 2.2
High-energy	$5.4 ± 1.2 \times 10^5$	32 ± 7
Pallet total dose		556 ± 37

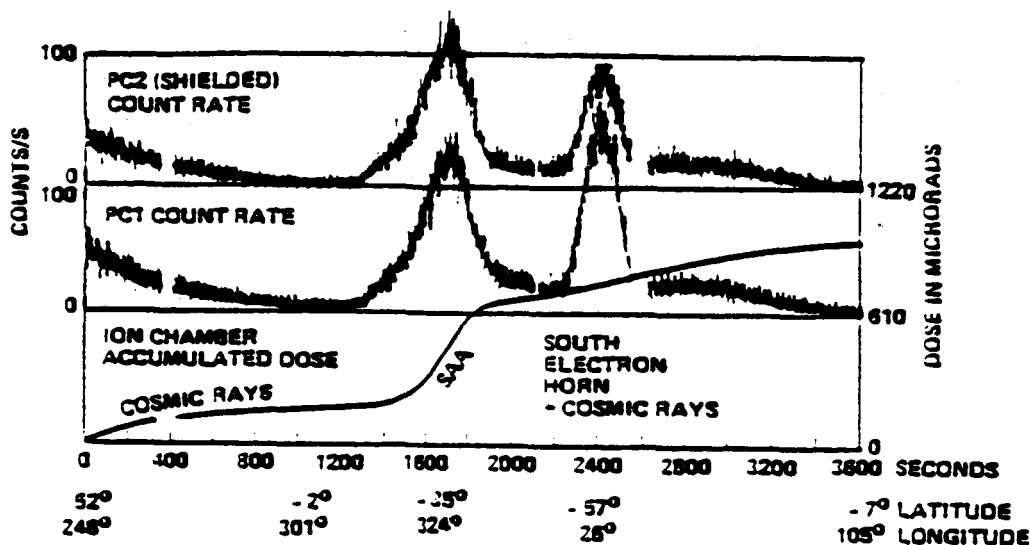*Dose in mrads. ‡ Note differences in CR-39 threshold on SL1 and SL2.

Fig. 2. Count rate of two proportional counters and ion chamber accumulation at high northern latitudes, the geomagnetic equator, the SAA, and the electron horn.

The segments of the ion chamber data indicating the SAA by temporal behaviour of the PC count rate comprise 0.13 of the average mission dose for the top ion chamber and 0.10 for the one in the bottom of rack 3. These small fractions may be somewhat biased by IC data gaps, but show clearly that the dose in the SL1 orbit is dominated by the cosmic rays, as predicted by pre-flight calculations /1/. The calculations also show that trapped protons would dominate above ~350-400 km for similar locations in the Spacelab module.

Occasionally at large geomagnetic latitudes, sudden increases in proportional counter rates occurred as shown in Figure 3. Bremsstrahlung photons of ~100 keV characteristic energy are indicated by the relative count rates of the shielded and unshielded proportional counters and the lack of significant dose rate above that expected from cosmic rays. The intensity was occasionally ~ twice that observed in the undisturbed south electron horn and episodes lasted from a few to ~500 seconds. Seventeen significant episodes occurred in the approximately five days of ARD data, more frequently near the end of the mission. These events resemble trapped electron "precipitation" events previously observed /10,11/, and work is in progress to classify them. This phenomenon may be significant for experimenters with photon sensitive instruments.
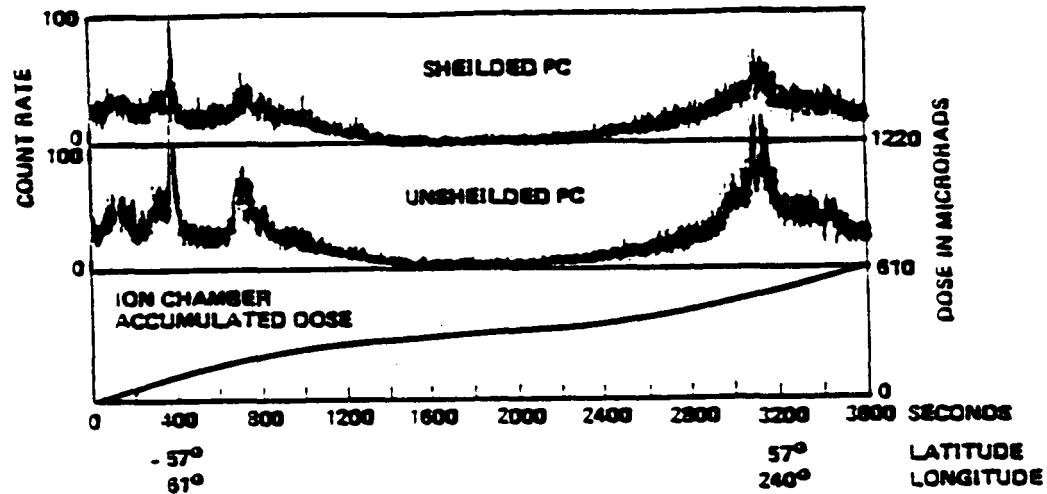
9

Fig. 3. One hour of ARD data in which the SAA and electron horns are not encountered. Large fluctuations in the PC count rates are due to bremsstrahlung photons.

The low fraction of dose due to trapped particles in the SL1 module makes assessment of the trapped environment and its absorbtion by shielding somewhat uncertain. Analysis is also complicated by the variation in attitude of the shuttle because the trapped particle angular distribution is directional with more particles arriving nearly perpendicular to magnetic field lines in a "pancake" distribution. To aid in assessing the SAA and south electron horn effects, contour maps of the radiation were assembled. Because of the short mission times and data gaps the maps were constructed by averaging data around geographical points (e.g., within 3°), and smoothing. Displayed in Figure 4 are the dose rate from two IC's and one of the PC's in the SAA region. That the two IC's are in different shielding situations is obvious. Comparisons between the IC and PC maps show high PC count rates in the south "electron horn" region, but the IC's have no significant dose accumulation there. This is due to the relatively high sensitivity of the PC's to bremsstrahlung photons as previously noted.

10

The averaging and smoothing in making the maps reduce count rates and dose rates actually observed near the center of the SAA. These values are found by taking maximum slopes of rates observed in direct data as shown in Figure 2. The maximum observed rates were about 20% higher than the map contours in the center of the anomaly.

The HZE heavy ion fluence was measured on SL1 with the CR-39 detectors that had a threshold sensitivity of LET_∞ = 40 keV/μm (relativistic Z = 15 at normal incidence to the CR-39). For SL2 the threshold was 8 keV/μm (Z = 7). With these detectors a track fluence at various locations between 125 $\pm$ 19 and 435 $\pm$ 59 particles/cm^2 were observed for the mission. The variations were most likely due to fragmentation of the heavy cosmic ray nuclei in varied shielding and shuttle attitudes, but no calculation has yet been done to verify this. An average of biological dose equivalent due to these particles is 18.5 $\pm$ 0.6 mrem/day in the SL1 module. On the SL1 pallet behind about 1 g/cm^2 minimum shielding the HZE fluences was 203 $\pm$ 26 particles/cm^2 for the mission, giving a biological dose of 14.2 $\pm$ 0.2 mrem/day. For Spacelab 2 the HZE fluence for the 3-day mission were 495 cm^{-2} and 489 cm^{-2} in the two PRD-P's, giving a dose equivalent of 34 $\pm$ 3 mrem/day for LET_∞(H_2O) > 3 keV/mrem.

The neutron fission foils produced data on thermal (<0.3 eV), resonance (0.3-1 MeV), and high energy (>1 MeV) neutrons. One set of fission foils in the SL1 module (PRD-M) measured mission fluences of 1.1 $\pm$ 1.1 x 10^4/cm^2 for thermal, 5.2 $\pm$ 1.6 x 10^5/cm^2 for resonance, and 7.1 $\pm$ 0.6 x 10^5/cm^2 for high energy neutrons. This gives a total module neutron dose of 4.4 $\pm$ 0.5 mrem/day. The respective values for pallet mounted PRD-P were 4.2 $\pm$ 1.3 x 10^4/cm^2, 1.5 $\pm$ 0.2 x 10^6/cm^2, 7.6 $\pm$ 0.7 x 10^5/cm^2, and 5.3 $\pm$ 0.3 mrem/dose, respectively. The errors are from track counting statistics. The neutron dose on the Spacelab 2 pallet was 4.2 $\pm$ 0.2 mrem/day.

11

4 (a)

Fig. 4. Maps of dose isocontours in the SAA for ion chambers 1 and 2. The PC count rate for the counter in ARD 1 (unshielded) is also shown. Dose rates for the ion chamber in the top of rack 3, shown in 4(a), are higher in the center of the SAA than for the one in the bottom of rack 3, shown in 4(b). The contours of the proportional counter 4(c) show high rates in the south horn, near longitude 30° E.

4 (b)

4 (c)

12
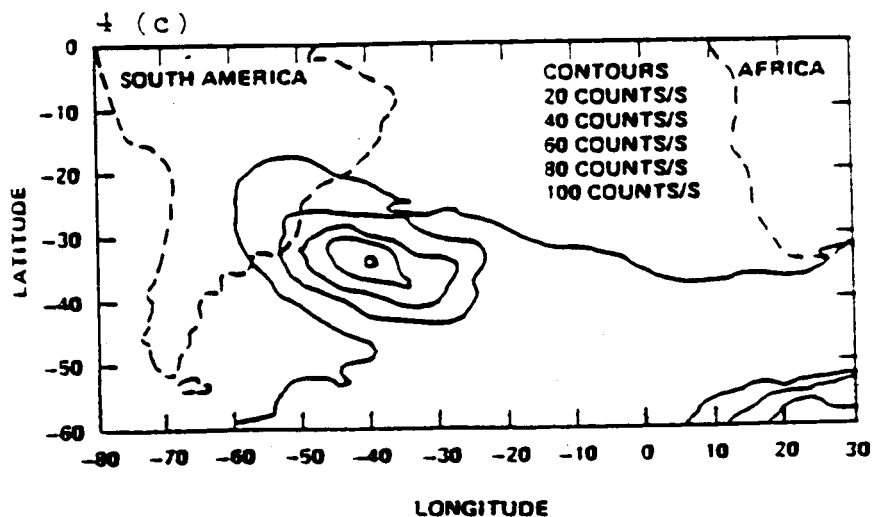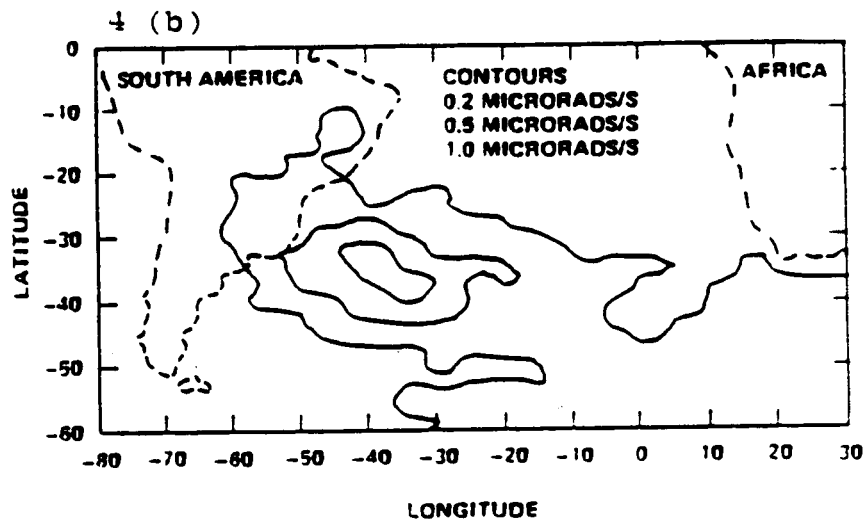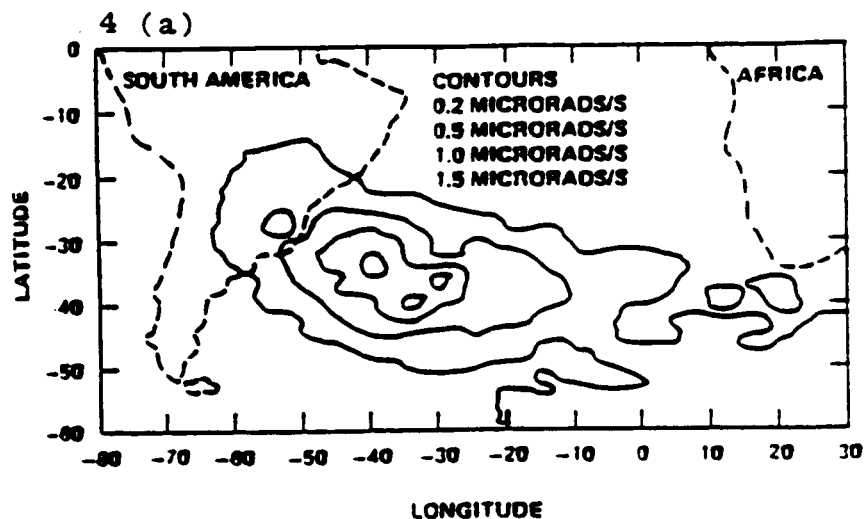
The sum of the low LET dose from the TLD's, the HZE dose, and the neutron dose gives the total biological dose equivalent. These were 33.0 ± 7.0 mrem/day for the SL1 module, 37.9 ± 4.6 mrem/day for the SL1 pallet, and 69.9 ± 4.6 mrem/day for the SL2 pallet. As has been previously pointed out /4,12/ the measure values of the low LET dose rate on SL1 are about twice as high as the dose measured on previous STS missions which were flown at similar altitudes but 28.5° inclination. The combined low and high LET rates (33 mrem day in the module) is about 3.5 times higher than the previous shuttle missions. This is a consequence of the much larger cosmic ray contribution to the dose at 57°.

Metal samples (Co, Ti, Ni, V) 5.0 cm square and 0.32 cm thick were included in two SL1 and one SL2 PRD's in order to measure activation of materials in the Spacelab/Shuttle environment. Gamma rays from activated spacecraft and detector systems are a major source of background in gamma ray astronomy. The samples were counted in a low-level gamma-ray spectrometer facility within 10 days of their return from orbit. The only activation isotope found to be well separated from the background was Co^{58} in a cobalt sample. A marginal detection of Co^{58} was found in the nickel sample. From Spacelab 2, the measured activity in the 73 gram cobalt sample was 70 ± 3 counts per 10^3 sec. Corrrecting for detector efficiency, self-absorption and decay following recovery, the activity at the end of the flight was 0.62 ± 0.06 dps/kg. The saturated activity, the activity which would have been reached if in orbit for much longer than the 71 day half-life of Co^{58}, is 5.9 ± 0.7 dps/kg. The activation found on Spacelab 1 was about one-third that of Spacelab 2. These low levels are due to the short mission time and low altitudes.

There are two main production modes for Co^{58} from the Co^{59} target: Co^{59} (p,pn) Co^{58} and Co^{58} (n,2n) Co^{58}. Although it is not possible to distinguish between the production modes, it is believed that the fluxes of activating neutrons and protons are comparable at the sample location. The cross sections for the above reactions are within a factor of two in the energy range of interest (≈20 MeV to 100 MeV). Using a mean cross section of 200 mb for the production of Co^{58}, the activating particle fluence is estimated to be

$5.2 \pm 0.7 \times 10^5/cm^{-2}$ for the mission. The total fluence of neutron from the fission foils plus protons from the nuclear track emulsions is ~$1.5 \times 10^6/cm^2$. Considering the low levels of activation and analysis uncertainties, the agreement is reasonable.

Comparison with Calculations and Discussion

The radiation environment to be anticipated within Spacelab was calculated in 1975 with the Earth's magnetic field extrapolated to 1980 /1/. The calculations included Vette's /13/ AP8 may trapped proton environment, the AE4-AE6 electron environment /16/ and the cosmic ray environment /17/. Calculations were made of radiation dose and proton and electron fluence for a simplified mass model of the Spacelab and for spherical shells.

When comparing the preflight predictions with the measurements an obvious difficulty is the complexity of the actual shielding distribution compared to the simplified ones used in the predictions. A second difficulty is that the doses for the SL1 and SL2 altitudes are dominated by the cosmic rays at shielding depths ≥ 2 g/cm^2 (where most of the detectors are), and thus measured dose is relatively insensitive to the trapped belt environment. The tables /1/ indicate that at spherical shielding depths of 10 g/cm^2 for SL1 the dose should be ~20 mrads/day, and at 40 g/cm^2, ~10 mrads/day. The measured average SL1 module dose was 10.0 mrads/day with the arithmetic average shielding depth for various detectors varying between 14 and 66 g/cm^2. On the SL1 pallet the PRD-P had a cover (insulation, aluminum housing, etc.) of 1.0 g/cm^2, but less than a 2π view of the sky. The tables would indicate about ~100 mrads/day if view angle and a 1 g/cm^2 spherical shield is considered. Electrons, followed by protons, would contribute most of the calculated dose. The PRD-P measurement was 18.9 mrad/day. The conclusions from the above comparisons were that the environment models used most likely overestimate the trapped particles, and that the simple shielding distributions were too simple for comparisons with measurements. We can also speculate that orbiter attitudes may have a large influence at thin shielding locations.

14

We have undertaken some recent calculations to illuminate the shielding distribution problem. For a sample of shielding locations in the SL1 module and in the tunnel we have used actual shielding distributions /14/ and defined a shielding measure, the "dose weighted depth," as described below. For the thinly shielded PRD-P's on SL1 and SL2, we have calculated dose from a "thin slab" model, since actual distributions from these locations were not yet available. We also calculated the expected count rate in the proportional counters due to bremsstrahlung X rays (from the trapped electrons). The remainder of this section describes these calculations and comparison with the measurements.

The relevant components to the charged particle radiation environment are the geomagnetically trapped protons and electrons, and the galactic cosmic ray nuclei. For these calculations the proton fluxes were obtained from the Vette proton model AP8MIN /13/ using the IGRF 1965 magnetic field model /15/ projected to 1964, the epoche of the flux model. The electron fluxes were obtained from AESMIN /16/ and the same field model. Galactic cosmic ray dose predictions which were taken from reference 17 include geomagnetic effects and ionization loss, and simplified corrections for interactions. Johnson Space Flight Center /14/ provided the mass distributions for 512 directions surrounding TLD locations from a geometrical model of the Shuttle and Spacelab. The calculations assume an isotropic primary particle flux, which would be the case for a long duration spinning spacecraft. It is only a rough approximation for Spacelab.

The results of dose calculations for the different radiation components are compared to the measured TLD doses in Table 2. This table contains only about 1/3 of the TLD locations, but represents the range of shielding thicknesses in the module and tunnel. The one on the pallet is discussed later.

The arithmetic average of the shield thicknesses along the 512 directions about the locations is in column 1. The spherical shell thickness that would result in the same

15

central dose as the calculated dose shown in column 6 is in column 2. This is called the "dose weighted depth." The dose weighted depth is dependent on the environmental models and orbital parameters. Column 3 is the dose due to electrons and bremsstrahlung calculated using techniques described in reference /18/. The electron dose fraction from each direction is approximated assuming an infinite plane shield of appropriate thickness for that direction. Columns 4 and 5 are the proton and galactic cosmic ray doses calculated in the "straight ahead" approximation /19/ through the shielding distribution. The total calculated dose is in column 6 and the measured TLD doses in column 7. The calculated values have not been corrected for the reduced sensitivity of the TLD's to heavy nuclei /9/. The calculated and measured doses from this table are shown in Figure 5.

TABLE 2   Spacelab 1 Shielding and Total Mission Dose at Sample
Locations in the Module and Tunnel

Arithmetic Average Shielding (g/cm^2)	Dose Weighted Average Shielding (g/cm^2)	Electron Dose (mrads)	Proton Dose (mrads)	Galactic Cosmic Ray Dose (mrads)	Total Dose (mrads)	Measured TLD Dose (mrads)
55	20	13	22	37	120	106.7 ± 2.7
14	6	4	57	110	170	122.3 ± 7.2
19	3	4	52	110	160	102.2 ± 2.7
23	3	56	62	110	220	142.9 ± 10.9
26	9	6	44	100	150	102.5 ± 3.5
26	3	49	58	100	210	141.0 ± 3.7
57	25	14	17	36	120	105.1 ± 3.8
34	12	18	26	100	140	104.3 ± 3.1
29	11	7	37	100	150	105.8 ± 2.6
56	30	3	15	31	100	109.2 ± 3.7
45	25	4	18	93	120	109.7 ± 2.6

The agreement between the predicted and measured doses is reasonable considering the isotropic flux assumption, the uncertainties in the environment models, and the shielding distribution approximations. Beyond about 10 g/cm^2 (dose weighted depth) the cosmic rays

16

contribute almost all of the dose. The three locations with the least shielding have higher doses than the rest due to trapped particles. The measurements are obviously lower than calculated at these locations indicating that the trapped environment models may predict too large a flux. The discrepancy between effective shield as defined by the arithmetic and dose weighted average shielding is noteworthy. Using the arithmetic average overestimates the effective shielding. For example the locations with weighted shielding of 3 g/cm^3 had shielding of between 1.0 and 1.5 g/cm^2 over ~3% of the total solid angle. Thus much of the difference between doses at these points and the rest is due to thin shielding over a small fraction of the solid angles. In Table 2 the electron component does not follow the dose weighted depth monotonically. This is because the electron contribution to the dose is a very steep function of shielded depth below 2 g/cm^2, and small solid angles with thin shielding have a large effect.
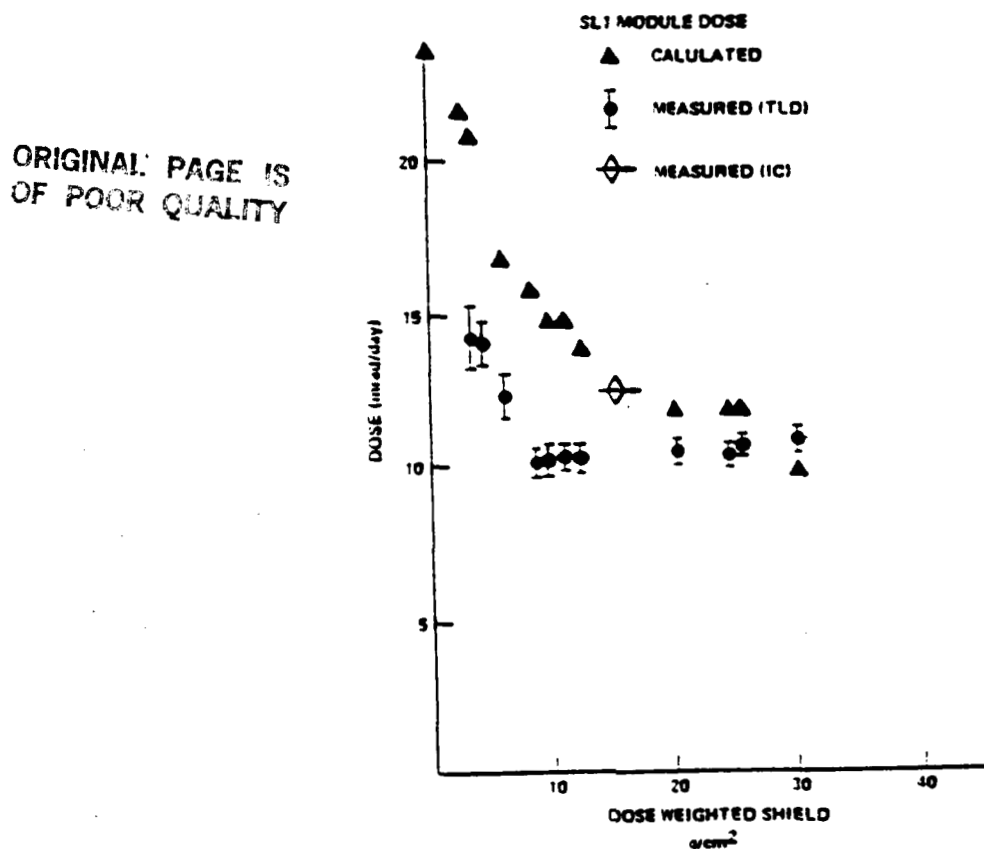
Fig. 5. Calculations using vector shielding of SL1 module radiation dose at 11 locations. The TLD and ion chamber measurements are also shown.

The TLD's in the packages on the Spacelab pallet were located inside the top of the cylindrical package. On Spacelab 1 the end cover over the TLD's was 1.0 g/cm^2 thick and on Spacelab 2 it was 1.25 g/cm^2. Vector shielding distributions were not available at these locations. The various components of the dose behind an infinite aluminum plane with infinite back shielding are shown in Table 3 for the Spacelab 1 and 2. The calculated Spacelab 1 dose behind 1.0 g/cm^2 is a factor of four higher than the measured pallet TLD dose of 18.9 mrad/day. The calculated Spacelab 2 dose behind 1.25 g/cm^2 interpolated from the table as 49 mrad/day is also higher than the 31 mrad/day observed.

TABLE 3 Dose Rates at a point Beneath an Infinite Plane of Aluminum with Infinitely Thick Back Shielding

Plane Thickness (g/cm^2)	Electron Dose (mrads/day)	Proton Dose (mrads/day)	Cosmic Ray Dose (mrads/day)	Total Dose (mads/day)
Spacelab 1 (250 cm 57°)				
0.5	530.0	7.4	6	540.0
1.0	68.0	5.1	6	79.0
1.5	7.1	4.1	6	17.0
2.0	0.70	3.5	6	10.0
3.0	0.34	2.7	6	9.0
40.0	0.0074	0.026	5	5.0
Spacelab 2 (315 cm 49.5°)				
0.5	300.0	33.0	5	340.0
1.0	41.0	24.0	5	70.0
1.5	4.4	19.0	5	28.0
2.0	0.38	16.0	5	21.0
3.0	0.16	13.0	5	18.0
40.0	0.0025	0.36	4	4.0

The thin slab dose values are calculated for infinite shielding behind the detectors. In the actual geometry some galactic cosmic rays would penetrate the structure below to add a contribution to the dose. The last table entry at 40 g/cm^2 is a rough estimate of this contribution through the "infinite" back.

18

The ARD packages each contained a shielded and unshielded proportional counter. The active region in each counter was 7 cm long and 2.5 cm in diameter and the shielding consisted of a copper sleeve 1.27 mm thick. The highest counter rates from the PC's were observed in the South Atlantic Anomaly and at high latitudes southeast of Africa where the south "horn" of the outer electron belt was encountered. Typical peak count rates were around 100 counts/sec in both regions. The estimated response of the proportional counters to bremsstrahlung in the center of the the south horn and the SAA are shown in Table 4. The bremsstrahlung photon spectrum behind an infinite plane slab of the given thickness was computed using the electron spectra shown in Table 5.

The electrons were assumed to be isotropically incident on the slab. The count rate was obtained by equation

$$C = A \int_E \phi(E) (1 - e^{-\mu(E)X}) dE$$

where $\phi(E)$ is the differential photon flux, $\mu(E)$ is the mass attenuation coefficient at photon energy E, A is the area of the detector, and X was the detector thickness. As a rough approximation, we took A as 2.5×7 cm^2, the area as seen from the side of a cylinder, and X as 2.5 cm. The calculated count rates (Table 4) in the "horn" are in fair agreement with the observed count rates. The calculated bremsstrahlung count rate from electrons in the SAA is ~ 2 orders of magnitude lower than observed, confirming that protons contribute almost all PC counts in the SAA. Figure 6 shows the bremsstrahlung photon spectrum as a function of planar shielding depth.

19

TABLE 4 Estimated Maximum Proportional Counter Rates due to Bremsstrahlung from Trapped Belt Electrons in the SL1 Orbit

Shielding Thickness (g/cm^2)	Horn Count Rate (Counts/s)	South Atlantic Anomoly Count Rate (Counts/s)
2.0	200	6
5.0	60	2
10.0	20	0.5

TABLE 5 Electron Integral Spectra for Spacelab 1 from AESMin at Epoche 1964

Electron Energy (MeV)	Electron Horn Max. Integral Flux (electron/cm^2-s)	South Atlantic Anomoly Max. Integral Flux (electron/cm^2-s)
0.05	4.08×10^5	1.37×10^5
0.25	1.93×10^5	1.39×10^4
0.5	1.01×10^5	2.57×10^3
1.0	4.70×10^4	4.68×10^2
1.5	1.93×10^4	1.80×10^2
2.0	7.93×10^3	7.99×10^2
2.5	3.53×10^3	3.36×10^1
3.0	1.44×10^3	4.69×10^0
3.75	1.27×10^2	0

Figure 6. Bremsstrahling Photon Energy Spectra Beneath Different Plane Shielding Thicknesses, Calculated Using The Electron Horn Maximum Flux In TABLE 5.

20
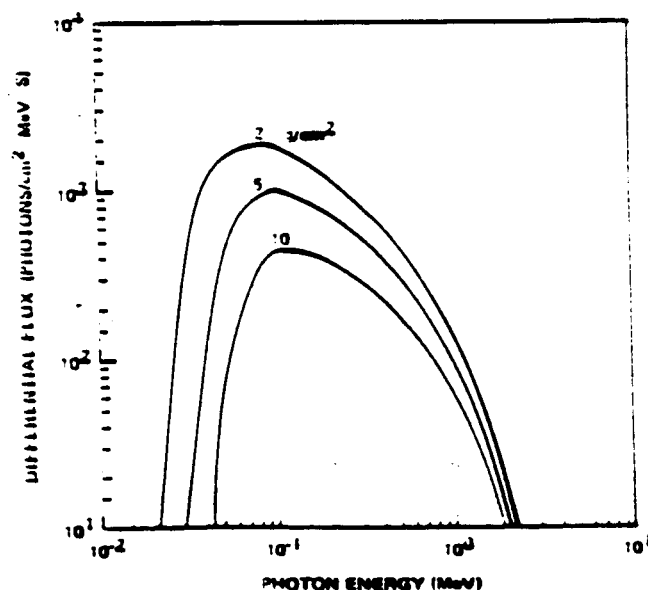
CONCLUSIONS

The large number of passive detectors at different locations, the measurement of the different environment constituents, and the temporal information from the active detectors presented an extensive, although not complete, survey of the radiation environment within Spacelab 1. Cosmic rays produced most of the dose at all locations in the Spacelab module. Only at a few detector locations was the dose significantly above that expected from the cosmic rays alone (Table 2, Figure 5). This was due to the large shielding depths ($\sim$14-56 g/cm^2 arithmetic average) of the Spacelab-Orbiter structure, and the low altitude. Detectors that had low shielding depths (< 1.5 g/cm^2) over significant solid angles registered the largest dose in the module. For these detectors, the fraction of the measured dose attributable to trapped particles is about 1/2 the calculated values. Shielding distributions for the least shielded detectors (Spacelab 1 and 2 pallet detectors) were not yet available. An infinite plane slab was used to calculate doses, which were a factor of 4 and 2 times those measured with the TLD's.

Comparison of the calculated doses with the set of TLD and ion chamber measurements (Tables 2 and 3, and Figure 4) indicate that the trapped fluxes from the models may be too large. Because the calculations use an omnidirectional flux, and the Spacelab 1 and 2 attitudes and short mission times may not fulfill this assumption, this tentative conclusion needs further testing.

The steep trapped electron and proton spectra cause small solid angles about detectors subtended by light shielding (< 2 g/cm^2) to dominate the trapped particle dose component. Thus a "dose weighted shield," calculated with the available trapped environment models was found convenient to place the measured doses in order with respect to shielding. For a massive spacecraft such as this, an accurate vector shield model is necessary before accurate doses can be predicted (e.g., for the space station cluster). For gravity gradient stabilized spacecraft the directional characteristics of the ambient

21

radiation may need to be considered. These considerations become more important at altitudes above 350-400 km where the trapped component becomes dominant.

The active detectors, although very simple, allowed separation of dose contributions from cosmic rays, trapped protons, and bremsstrahlung from electrons. These measurements indicated that 85-90% of the radiation dose in the Spacelab 1 module was caused by cosmic rays; that almost all module dose in the SAA is from protons; and that high energy X-rays caused by trapped electrons in the "south horn region" are intense but cause little of the dose. Unexpectedly frequent occurrences of bremsstrahlung photon "bursts," apparently from electrons "precipitating" from the trapped belt were observed. The ion chamber mission dose (128 mrad) and the TLD dose (109 mrad) are consistent if the TLD results are corrected for relative insensitivity to heavy ions.

The HZE particle flux measurements with the CR-39 track detectors indicate a large equivalent dose from these particles, as expected from the large cosmic ray contribution. The low LET dose was a factor of 2 and the dose equivalent a factor of 3.5 that observed at 28.5° and similar altitudes.

The observed total neutron fluence ($\sim 1.2 \times 10^5$ cm^{-2}) in the module and $\sim 2.3 \times 10^5$ cm^{-2} on the pallet) were about 2.5 to 5 times the charged particle fluence measured with nuclear track emulsions. This is compatible with measurements in Skylab /20/, which had a similar spacecraft mass and inclination, but higher altitude.

The detectors used here give no information about some aspects of the environment such as the energy spectra of individual charged particle species, or e.g., temporal variations of neutrons. However, this ensemble of passive and active detectors has given good survey of the radiation constituents in a complex spacecraft and indicates the advantages and efficiency of coordinated measurements with passive and active detectors. These measurements and calculations indicate the complexity of accurately predicting all

22

relevant radiation phenomena for future Spacelab users, as well as Space Station experimenters and crews.

ORIGINAL PAGE IS
OF POOR QUALITY

REFERENCES

1. Watts, J. W., Jr., and J. J. Wright, "Charged Particle Radiation Environment for the Spacelab and Other Missions in Low Earth Orbit - Revision A" - NASA TMX-73358.

2. "Spacelab Mission 1 Experiment Descriptions," pV-39, Paul Craven editor, NASA TM 78173 (1978)

3. "ENVO1 Measurement Description," unpublished, available from Thomas A. Parnell (1978)

4. Benton, E. V., A. L. Frank, T. A. Parnell, J. W. Watts, Jr., and J. C. Gregory, AIAA Conference Proceedings #859, Paper 85-7045-CP (1985).

5. Benton, E. V., R. M. Cassore, A. L. Frank, R. P. Henke, and D. D. Peterson, "Space Radiation Dosimetry on board COSMOS-936: US Portion of Experiment K-206," University of San Francisco Report TR-48 (1981).

6. Benton, E. V., R. P. Henke, A. L. Frank, C. S. Johnson, R. M. Cassore, M .T. Tran, and E. Etter, "Space Radiation Dosimetry Aboard COSMOS 1129: Experiment K-309," University of San Francisco Report TR-53 (1981).

7. Digital Data Dosimetry, Tulsa, OK, Model 1/E-1

8. Reuter Stokes, Cleveland, OH, Model RS-P3-0803-287

9. Benton, E. V., and A. L. Frank, Data on Calibration of TLD's to heavy ions

10. Imhof, W. L., J. B. Reagan, G. H. Nakano, and E. E. Gaines, J. Geophys. Res, $\underline{84}$, 6371 (1979)

11. Imhof, W. L., et al., Journal of Geophysical Research, $\underline{91.A3}$, 3077 (1986).

12. Benton, E. V., and R. P. Henke, Space Research (1983).

13. Sawyer, Donald M., and James I. Vette, "AP-8 Trapped Proton Environment for Solar Maximum and Solar Minimum", NSSDC 74-03, April 1974.

14. Hardy, Alva and William Atwell, JSC, private communications.

15. Cain, Joseph C., and Shirley J. Cain, "Derivation of the International Geomagnetic Reference Field" (IGRF 10/68), NASA Technical Note T ND-6237, August 1971. Stassinopoulos, E. G., and D. Gilbert Mead, "ALLMAG, GDALMG, LINTRA: Computer Programs for Geomagnetic Field and Field-Line Calculations", NSSDC 72-12, February 1972.

16. Teague, Michael J., and James I. Vette, "A Model of the Trapped Electron Population for Solar Minimum", NSSDC 74-03, April 1974.

17. Burrell, M. O., and J. J. Wright, "The Estimation of Galactic Cosmic Ray Penetration and Dose Rates", NASA Technical Note TN D-6600, March 1972.

18. Watts, J. W., Jr., and M. O. Burrell: "Electron and Bremsstrahlung Penetration and Dose Calculation", NASA TND-6385, June 1971.

19. Burrell, M. O., "The Calcuation of Proton Penetration and Dose Rates", NASA TM-X-53063, August 25, 1964.

20. Fishman, G. J., Advances in Aeronautics and Astronautics 48, 397 (1976); Fishman, G. J., and C. A. Meegan, NASA TM-78263 (1980).